Proceedings of the 22th National and 11th International ISHMT-ASME Heat and Mass Transfer Conference December 28-31, 2013, IIT Kharagpur, India

HMTC1300415

ACTIVE DAMPING OF SMART FUNCTIONALLY GRADED SANDWICH PLATES UNDER THERMAL ENVIRONMENT USING 1-3 PIEZOELECTRIC COMPOSITES

R. Suresh Kumar
Dept. of Mechanical Engineering
Indian Institute of Technology
Kharagpur (WB) 721302, India
rsureshiitkgp@mech.iitkgp.ernet.in

S. I. Kundalwal
Dept. of Mechanical Engineering
Indian Institute of Technology
Kharagpur (WB) 721302, India
sikundalwal@iitkgp.ac.in

M. C. Ray
Dept. of Mechanical Engineering
Indian Institute of Technology
Kharagpur (WB) 721302, India
mcray@mech.iitkgp.ernet.in

ABSTRACT

The present study is concerned with the active control layer damping (ACLD) of the geometrically nonlinear vibrations of the smart functionally graded (FG) sandwich plates subjected to the thermal loading. The constraining layer of the ACLD treatment is considered to be made of the vertically/obliquely reinforced 1-3 piezoelectric composite (PZC) while the viscoelastic material is modeled by using the Golla–Hughes–McTavish (GHM) method in the time domain. A three dimensional coupled nonlinear electromechanical finite element (FE) model has been developed based on the first order shear deformation theory (FSDT) and Von Karman type nonlinear strain displacement relations to investigate the damping characteristics of the FG sandwich plates subjected to the thermal loading. Several FG sandwich plates with different thermal loading conditions have been investigated to evaluate the numerical results. Effects of metal or ceramic rich bottom surfaces subjected to the thermal loading, the variation of power-law index on the control authority of the ACLD patches have been thoroughly investigated. Emphasis has also been placed on investigating the effect of the variation of piezoelectric fiber orientation angle on the performance of the ACLD patches for controlling the geometrically nonlinear transient responses of FG sandwich plates.

LIST OF ABBREVIATIONS

ACLD	Active Constrained Layered Damping
FGM	Functionally Graded Material
FE	Finite Element
FSDT	First Order Shear Deformation Theory
PZC	Piezoelectric Composite
GHM	Golla-Hughes-McTavish

NOMENCLATURE

a	Length (m) of the sandwich plate
b	Width (m) of the sandwich plate
H	Thickness of the substrate sandwich plate
V	Applied control voltage
h	Thicknesses of the top and bottom facing
h_c	Half the thickness of the core
h_v	Thickness of the viscoelastic layer
h_p	Thickness of the 1-3 PZC layer
r	Power law index
m	Number of ACLD patches
I_d	Performance index
Ψ	Piezoelectric fiber orientation angle (deg) in the 1-3 PZC layer
x, y, z	Cartesian coordinates
u_0, v_0, w_0	Translational displacements (m) at any point on the mid plane along x, y and z directions
(u_c, v_c, w_c)	Displacement fields x, y and z directions, respectively at any point in the core
(u_b, v_b, w_b)	Displacements x, y and z directions at any point in the bottom facing
(u_t, v_t, w_t)	Displacements x, y and z directions at any point in the top facing
(u_v, v_v, w_v)	Displacements x, y and z directions at any point in the viscoelastic layer
(u_p, v_p, w_p)	Displacement x, y and z directions at any point in the 1-3 PZC layer
$\theta_x, \phi_x, \alpha_x, \beta_x, \gamma_x$	Rotations (rad) of the normals about the mid planes of each layer about the $y-$ axis

$\theta_y, \phi_y, \alpha_y, \beta_y, \gamma_y$	Rotations (rad) of the normals about the mid planes of each layer about the $x-$ axis
$\theta_z, \phi_z, \alpha_z, \beta_z, \gamma_z$	Gradients (rad) of the transverse deformations of each layer about the $z-$ axis
$\varepsilon_x, \varepsilon_y, \varepsilon_z$	Normal strains
$\varepsilon_{xy}, \varepsilon_{yz}, \varepsilon_{zx}$	In-plane and out of plane transverse shear strains
$\sigma_x, \sigma_y, \sigma_z$	Normal stresses
$\sigma_{xy}, \sigma_{yz}, \sigma_{zx}$	In-plane and out of plane transverse shear stresses
ρ, ρ_m, ρ_c	Densities of the flexible core, metal and ceramic materials
$\upsilon, \upsilon_m, \upsilon_c$	Poissons' ratios of the core, metal and ceramic materials
V^k $(k = 1, 2\ and\ 3)$	Volume fraction of the bottom layer, the core and the top layer of the substrate FG sandwich plate
E_m, E_c	Young's modulus of the metal and the ceramic materials
$[C_b]_m, [C_s]_m$	Elastic coefficient matrix for the metal and the core
$[C_b^c], [C_s^c]$	Elastic coefficient matrix for the core
$[C_b]_p, [C_{bs}]_p$	Elastic coefficient matrix and elastic coupling constant matrix for the 1-3 PZC layer
$e_b, e_s \in_{ij}$	The piezoelectric coefficient matrix and the dielectric matrix for the 1-3 PZC layer
D_z, E_z	Electric displacement and Electric field along $Z-$axis
P, K_d	Applied mechanical load (N/m^2), control gain
T_p, T_k	The potential energy and the kinetic energy of the overall plate
$\mathrm{T_p^e}, \mathrm{T_k^e}$	The potential and the kinetic energy of element integrated with a patch of the ACLD treatment
δ	Variational operator
A, Ω	Surface area and the Volume of the smart FG plate
a^e, b^e	Elemental length and width under consideration
$\{\mathrm{d_t}\}, \{\mathrm{d_r}\}$	Elemental displacement vectors
$[\mathrm{N_t}], [\mathrm{N_r}]$	Nodal shape function matrices
$\{\mathrm{d_t^e}\}, \{\mathrm{d_r^e}\}$	Nodal displacement vectors
$\mathrm{n_i}$	Shape function associated with the i^{th} node
$\{\varepsilon_b\}_c, \{\varepsilon_b\}_t, \{\varepsilon_b\}_b, \{\varepsilon_b\}_p$ $\{\varepsilon_s\}_c, \{\varepsilon_s\}_b, \{\varepsilon_s\}_t, \{\varepsilon_s\}_v, \{\varepsilon_s\}_p$	Elemental strains vectors expressed in terms of nodal displacement vectors
$[\mathrm{B_{tb}}], [\mathrm{B_{rb}}], [\mathrm{B_{ts}}], [\mathrm{B_{rs}}],$ $[\mathrm{B_1}], [\mathrm{B_2}]$	Nodal strain displacement vectors
$[\mathrm{K_{tt}^e}], [\mathrm{K_{tr}^e}], [\mathrm{K_{rt}^e}], [\mathrm{K_{rr}^e}]$ $[\mathrm{K_{tsv}^e}], [\mathrm{K_{trsv}^e}], [\mathrm{K_{rrsv}^e}]$	Elemental stiffness matrices
$[\mathrm{K_{tt}}], [\mathrm{K_{tr}}], [\mathrm{K_{rt}}], [\mathrm{K_{rr}}],$ $[\mathrm{K_{tsv}}], [\mathrm{K_{trsv}}]\ [\mathrm{K_{rrsv}}]$	Global stiffness matrices
$\{\mathrm{F_{tp}^e}\}, \{\mathrm{F_{tpn}^e}\}, \{\mathrm{F_{rp}^e}\}$	Elemental electro-elastic coupling matrices
$\{\mathrm{F_{tp}}\}, \{\mathrm{F_{tpn}}\},\ \{\mathrm{F_{rp}}\}$	Global electro- elastic coupling vectors
$\{\mathrm{F}\}, \{\mathrm{F^e}\}$	Global nodal load vector and elemental load vector
$[\mathrm{M}], [\mathrm{M^e}]$	Global mass matrix and elemental mass matrix
$\{\mathrm{X_t}\},\ \{\mathrm{X_r}\}$	Vectors of translational and rotational global nodal degrees of freedom
$\mathcal{L}$	Laplace operator
$\{\tilde{\mathrm{X}}_\mathrm{t}\}, \{\tilde{\mathrm{X}}_\mathrm{r}\}, \{\tilde{\mathrm{F}}\}$	Laplace transforms of vectors of translational, vectors of rotational global nodal degrees of freedom and global nodal load vector
$G(t)$	Material relaxation function of the viscoelastic material
$\mathrm{s}\widetilde{\mathrm{G}}(\mathrm{s})$	Material modulus function
$G^\infty,\ \alpha_k, \widehat{\omega}_k, \hat{\xi}_k$	GHM parameters
$\mathrm{Z}, \mathrm{Z_r}$	Auxiliary dissipation coordinates
$\tilde{\mathrm{Z}}(\mathrm{s}), \tilde{\mathrm{Z}}_\mathrm{r}(\mathrm{s})$	Laplace transforms of the auxiliary dissipation coordinates
Ω (ω_{NL}/ω_L)	Frequency (rad/s) Nonlinear fundamental frequency ratio
$[\mathrm{C_d}^*]$	Active damping matrix

INTRODUCTION

Amongst all possible existing composite structures, the idea of sandwich construction has become increasingly popular over the last three decades in aerospace, automobile, locomotive and construction industries because of the development of man-made cellular materials as core materials. The configuration of sandwich structure is a three-layer type of construction in which a light weight, thick flexible core is sandwiched between two stiff, strong face sheets [1-9]. The face sheets are basically made up of unidirectional orthotropic laminated FRP composites, while the core is thick layer of low-density material like foam polymer or honeycomb material made of resin-impregnated aramid paper (Nomex or Kevlar) [7]. The separation of the face sheets by the core increases the moment of inertia of the structure thereby producing an efficient structure for resisting bending and buckling loads. The strength and the stiffness of sandwich construction are increased without an appreciable increase in the corresponding weight of the structure [4]. However, the abrupt change in material properties across the interface layers may result in the development of high interlaminar stresses which may lead to the debonding of the interfacial layers. In order to alleviate such adverse effects, a new class of non-homogenous composite materials known as "functionally graded materials (FGMs) has earned a considerable attention in structural applications. These materials are characterized by a continuous variation of material properties particularly along the thickness direction which eliminates the occurrence of interface debonding between the layers. Yamanouchi et al. and Koizumi [10, 11] developed these novel materials where the continuous variation of material properties is a result of the change of composition and structure over the volume. The simplest form of FGMs is where two different material ingredients change gradually along the thickness of the structure from one to the other. Typically, FGMs are made from a mixture of ceramic and metal or a combination of different materials owing to their applications. The ceramic composition in the FGM offers thermal resistance while the metallic composition toughens and strengthens the structure.

A great deal of research has been carried out to analyse the behaviour of the structures made of FGMs. Feldman and Aboudi [12] carried out the buckling analysis of the FG plates subjected to uni-axial loading. Loy et al., [13] have studied the vibration of FG cylindrical shells using Love's shell theory. Zenkour [14] studied the bending analysis of laminated and sandwich elastic beams by the transverse shear and the normal deformation theory. Reddy [15] presented the solutions for the FG rectangular plates using his third order shear deformation theory. Sankar [16] derived the elastic solutions for the FG beam using a simple Euler Bernoulli beam theory. Vel and Batra [17] have presented an exact three-dimensional solution for the thermoelastic deformations of FG simply-supported plates of finite dimensions. Zenkour [18] developed generalized shear deformation theory for bending analysis of FG plates considering the Layerwise model and the symmetry of the plate about the mid-plane. Zenkour [19, 20] also carried out the stress and the vibration analyses of the FG sandwich plates with face layers being made of non-homogeneous isotropic ceramic-metal FGMs while the core layer is made of a homogenous ceramic material.

Over the past few decades, the use of piezoelectric materials for achieving the active control of the engineering structures has been the focus of many researchers. The converse and the direct piezoelectric effects of piezoelectric materials are exploited to use them as distributed actuators and sensors. Flexible structures integrated with such piezoelectric sensors and actuators possess self-monitoring and self-controlling capabilities and are customarily known as "smart structures" [21-26]. The major drawbacks of the existing monolithic piezoelectric materials is that the magnitudes of their piezoelectric coefficients are very low and hence, large control voltage is necessary to achieve significant control of vibrations of host structures. Subsequently, research devoted to the efficient use of these low-control-authority monolithic piezoelectric materials led to the development of active constrained layer damping (ACLD) treatment [27]. In ACLD treatment, the constrained layer is made of viscoelastic material while the constraining layer is made of piezoelectric material which may be active or passive under operation damping the host structure. When the treatment is integrated with a base structure (substrate) and its constraining layer is activated with an appropriate control voltage, the transverse shear deformations of the viscoelastic layer are enhanced causing improved damping characteristics of the overall structure. If the constraining layer is not activated, the treatment plays the role of passive constrained layer damping (PCLD) treatment. Thus the ACLD treatment provides the attributes of both active and passive damping. Hence, the ACLD treatment has gained tremendous importance for efficient and reliable active control of flexible smart structures.

Piezoelectric composite (PZC) materials [28-32] have now emerged as new class of smart materials having wide range of effective material properties which are not offered by the existing monolithic piezoelectric materials. In PZCs, the reinforcements are made of the existing monolithic piezoelectric materials and the matrix is the conventional epoxy. Among the various PZC materials studied by the researchers till today, laminae of the vertically/obliquely reinforced 1–3 PZC materials are commercially available [30] and are being effectively used in medical imaging applications and high frequency underwater transducers. The constructional feature of a layer of the vertically/obliquely reinforced 1–3 PZC material is illustrated in Fig. 1(a) where the reinforcing piezoelectric fibers are coplanar with the vertical $xz-$ or $yz-$plane making an angle Ψ with respect to the $z-$axis while the fibers are poled along their length. For the vertically reinforced 1–3 PZC the value of Ψ is zero and in case of the obliquely reinforced 1–3 PZC its value is nonzero.

Flexible sandwich structures are prone to undergo large amplitude vibrations due to very low internal damping. Extensive studies on the large amplitude free vibrations of composite sandwich structures and FG structures using approximate analytical and finite element methods have been reported by many researchers [33-39]. However, very few studies concerning the geometrically nonlinear dynamic analysis of smart composite and FG structures are available. Pai et al. [40] developed a refined model for nonlinear analysis of composite plates integrated with piezoelectric sensors and actuators. Ray and Baz [41] developed a variational model to investigate the control of nonlinear vibrations of beams using ACLD treatment. Reddy and Cheng [42] carried out a three dimensional analysis of smart FG plates. Kulkarni and Bajoria [43] derived a FE model based on the higher order shear

deformation theory for the geometrically nonlinear analysis of smart thin and sandwich plates. Panda and Ray [44] studied the nonlinear static behavior of the FG plates integrated with a layer of horizontally reinforced piezoelectric fiber reinforced composite. Although the piezoelectric actuator layer acts more efficiently as the constraining layer of the ACLD treatment, researchers did not pay much attention to the use of the ACLD treatment for controlling the nonlinear vibrations of composite sandwich and FG structures. Recently, Panda and Ray [45] investigated the performance of a proposed horizontally reinforced PZC, commercially not available yet, as the material of the constraining layer of the ACLD treatment for active damping of nonlinear vibrations of FG plates. Sarangi and Ray [46] carried out ACLD of geometrically nonlinear vibrations of laminated composite beams using vertically/obliquely reinforced 1-3 PZC material as the constraining layer. Most recently Kumar and Ray [47] derived a FE model for the geometrically nonlinear vibrations of composite sandwich plates integrated with the ACLD patches using layerwise FSDT model. The above study by Kumar and Ray [47] motivated the authors to report the effect of the performance of the ACLD patches on geometrically nonlinear vibrations of FG sandwich plates made of FG facings separated by homogenous isotropic core ceramic core/flexible HEREX core. The dynamic characteristics of the FG sandwich plates with non-homogenous isotropic FG top and bottom face layers separated by a homogenous isotropic ceramic core [20] or flexible HEREX core [4] may be different from that of the conventional FG plates. Hence, the necessity for the further study on the ACLD of geometrically nonlinear vibrations of FG sandwich plates arises. However, no work is reported yet on the ACLD of geometrically nonlinear vibrations of FG sandwich plates using vertically/obliquely reinforced 1–3 PZC materials.

In the present investigation, the performance of the ACLD treatment using vertically/obliquely reinforced 1-3 PZC material as the material of the constraining layer of the ACLD treatment for active damping of geometrically nonlinear vibrations of FG sandwich plates has been studied. The top and the bottom faces of the sandwich plate are made of FGMs whose properties vary along the thickness according to a power law distribution in terms of the volume fraction of the constituents while the core may be a hard or a soft material. A three dimensional finite element model has been developed for the FG sandwich plates integrated with the patches of the ACLD treatment. The viscoelastic layer of the ACLD treatment has been modeled using the Golla–Hughes–McTavish (GHM) method [48-50]. Several substrate FG sandwich plates with different core materials are considered for presenting the numerical results. The nonlinear fundamental frequency ratios of the FG sandwich plates with different configurations have been estimated. Also, the effect of variation of the piezoelectric fiber orientation angle (Ψ) in the 1–3 PZC constraining layer on the control authority of the ACLD patches has been investigated.

GOVERNING EQUATIONS

Figure.1 (b) illustrates a schematic diagram of a smart FG sandwich plate in which the substrate FG sandwich plate is considered to be symmetric about the mid plane. The top and the bottom facings of the sandwich plate are composed of non-homogenous isotropic two constituent ceramic-metal FGMs whose material properties like modulus of elasticity and poissons ratio vary across the thickness based on a standard power law which is a function of volume fractions of the constituents while the core of the sandwich plate is a flexible isotropic HEREX honeycomb (soft) structure. The top surface of the top facing of the sandwich plate is integrated with the patches of the ACLD treatment. The constraining layer of the ACLD treatment is composed of the vertically/obliquely reinforced 1-3 PZC layer illustrated schematically in Fig. 1(a).

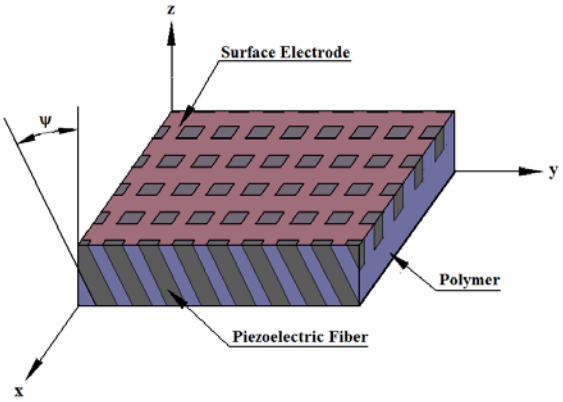

(a)

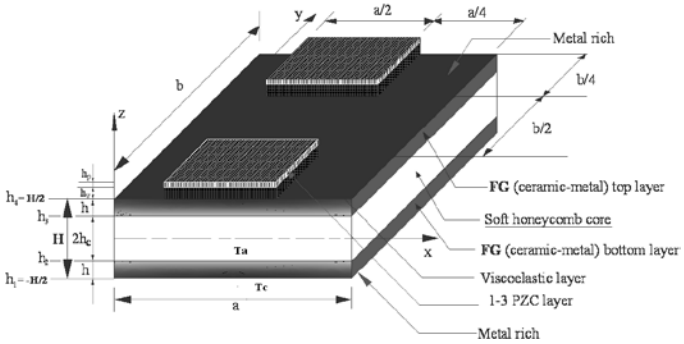

(b)

Figure 1. SCHEMATIC DIAGRAMS OF (a) LAMINA OF VERTICALLY ($\Psi = 0$)/OBLIQUELY ($\Psi \neq 0$) REINFORCED 1-3 PZC MATERIAL AND (b) FG SUBSTRATE PLATE INTEGRATED WITH THE ACLD PATCHES.

The length, the width and the thickness of the substrate sandwich plate are denoted by a, b and H, respectively. The thickness of the constraining 1-3 PZC layer and the constrained viscoelastic layer of the ACLD treatment are h_p and h_v, respectively. The thickness of each facing and half of the thickness of the core are h and h_c, respectively. The origin of the rectangular Cartesian coordinate system (xyz) is fixed at one corner of the mid-plane of the core, such that the lines $x = 0$ and a and $y = 0$ and b represent the boundaries of the mid-plane of the core. Since, the elastic properties of the adjacent continua of the overall sandwich structure differ in orders, each layer of the sandwich plate is modeled separately using FSDT to study the kinematics of deformations of the overall sandwich structure. Figures 2(a) and 2(b) illustrate the kinematics of deformations of the undeformed transverse normal in the $xz-$ and the $yz-$ planes, respectively.

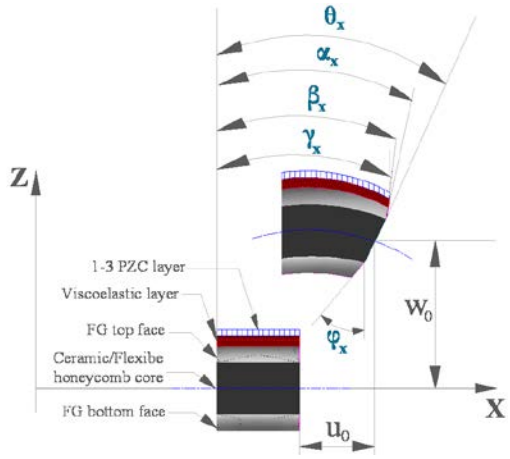

(a)

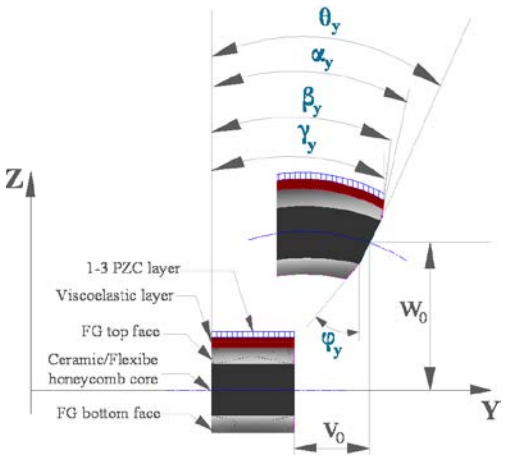

(b)

Figure 2. KINEMATICS OF DEFORMATION

As shown in this figure, u_0, v_0 and w_0 represent the generalized translational displacement of a point along the mid-plane of the core, $\theta_x, \phi_x, \alpha_x, \beta_x$ and γ_x represent the rotations of the portions of the normal lying in the core, the bottom layer, the top layer, the viscoelastic layer and the piezoelectric layer, respectively in the $xz-$plane while θ_y, ϕ_y, α_y, β_y and γ_y represent the same in the $yz-$plane. Thus the five sets of displacement fields describing the kinematics of deformations while satisfying the interface continuity conditions between the adjacent layers can be expressed as follows:

The displacement u_t , v_t and w_t along x, y and z directions, respectively at any point in the top layer are

$$u_t(x,y,z,t) = u_0(x,y,t) + h_c\theta_x(x,y,t) + (z-h_c)\alpha_x(x,y,t)$$
$$v_t(x,y,z,t) = v_0(x,y,t) + h_c\theta_y(x,y,t) + (z-h_c)\alpha_y(x,y,t)$$
$$w_t(x,y,z,t) = w_0(x,y,t) + h_c\theta_z(x,y,t) + (z-h_c)\alpha_z(x,y,t) \quad (1)$$

The displacement u_b , v_b and w_b along x, y and z directions, respectively at any point in the bottom layer are

$$u_b(x,y,z,t) = u_0(x,y,t) - h_c\theta_x(x,y,t) + (z+h_c)\phi_x(x,y,t)$$
$$v_b(x,y,z,t) = v_0(x,y,t) - h_c\theta_y(x,y,t) + (z+h_c)\phi_y(x,y,t)$$
$$w_b(x,y,z,t) = w_0(x,y,t) - h_c\theta_z(x,y,t) + (z+h_c)\phi_z(x,y,t) \quad (2)$$

The displacement fields u_c , v_c and w_c along x, y and z directions, respectively at any point in the core are

$$u_c(x,y,z,t) = u_0(x,y,t) + z\theta_x(x,y,t)$$
$$v_c(x,y,z,t) = v_0(x,y,t) + z\theta_y(x,y,t)$$
$$w_c(x,y,z,t) = w_0(x,y,t) + z\theta_z(x,y,t) \quad (3)$$

The displacement fields u_v , v_v and w_v along x, y and z directions, respectively at any point in the viscoelastic layer are

$$u_v(x,y,z,t) = u_0(x,y,t) + h_c\theta_x(x,y,t) + h\alpha_x(x,y,t) + (z-h_4)\beta_x(x,y,t)$$
$$v_v(x,y,z,t) = v_0(x,y,t) + h_c\theta_y(x,y,t) + h\alpha_y(x,y,t) + (z-h_4)\beta_y(x,y,t)$$
$$w_v(x,y,z,t) = w_0(x,y,t) + h_c\theta_z(x,y,t) + h\alpha_z(x,y,t) + (z-h_4)\beta_z(x,y,t) \quad (4)$$

The displacement fields u_p , v_p and w_p along x, y and z directions, respectively at any point in the 1-3 PZC layer are

$$u_p(x,y,z,t) = u_0(x,y,t) + h_c\theta_x(x,y,t) + h\alpha_x(x,y,t) + h_v\beta_x(x,y,t) + (z-h_5)\gamma_x(x,y,t)$$
$$v_p(x,y,z,t) = v_0(x,y,t) + h_c\theta_y(x,y,t) + h\alpha_y(x,y,t) + h_v\beta_y(x,y,t) + (z-h_5)\gamma_y(x,y,t)$$
$$w_p(x,y,z,t) = w_0(x,y,t) + h_c\theta_z(x,y,t) + h\alpha_z(x,y,t) + h_v\beta_z(x,y,t) + (z-h_5)\gamma_z(x,y,t) \quad (5)$$

In Eqs. (1) - (5), the variables θ_z, ϕ_z, α_z, β_z *and* γ_z represent the gradients of the transverse normal displacements at any point in the core, the bottom layer, the top layer, the viscoelastic layer and the piezoelectric layer, respectively. For the ease of analysis and computation, the translational displacement variables are separated from other variables as follows:

$\{\mathbf{d_t}\} = [u_0\ v_0\ w_0]^T$ and

$$\{\mathbf{d_r}\} = \left[\theta_x\ \theta_y\ \theta_z\ \phi_x\ \phi_y\ \phi_z\ \alpha_x\ \alpha_y\ \alpha_z\ \beta_x\ \beta_y\ \beta_z\ \gamma_x\ \gamma_y\ \gamma_z\right]^T \quad (6)$$

The state of strain at any point in the overall plate is divided into the bending strain vector $\{\boldsymbol{\varepsilon_b}\}$ and the out of plane shear strain vector $\{\boldsymbol{\varepsilon_s}\}$ as follows:

$$\{\boldsymbol{\varepsilon}_b\} = \{\varepsilon_x\ \varepsilon_y\ \varepsilon_{xy}\ \varepsilon_z\}^T \text{ and } \{\boldsymbol{\varepsilon}_s\} = \{\varepsilon_{xz}\ \varepsilon_{yz}\}^T \quad (7)$$

where, $\varepsilon_x, \varepsilon_y, \varepsilon_z$ are the normal strains along x, y and z directions, respectively; ε_{xy} is the in-plane shear strain and $\varepsilon_{xz}, \varepsilon_{yz}$ are the transverse shear strains. By using the displacement fields and the von Kármán type of nonlinear strain-displacement relations, the strain vectors $\{\boldsymbol{\varepsilon}_b\}_c, \{\boldsymbol{\varepsilon}_b\}_b$, $\{\boldsymbol{\varepsilon}_b\}_t$, and $\{\boldsymbol{\varepsilon}_b\}_p$ defining the state of in-plane and transverse normal strains at any point in the core, the bottom layer, the top layer and the active constraining layer, respectively, can be expressed as:

$$\{\boldsymbol{\varepsilon}_b\}_c = \{\boldsymbol{\varepsilon}_{bt}\} + [\mathbf{Z}_1]\{\boldsymbol{\varepsilon}_{br}\} + \{\boldsymbol{\varepsilon}_{bnr}\},$$
$$\{\boldsymbol{\varepsilon}_b\}_b = \{\boldsymbol{\varepsilon}_{bt}\} + [\mathbf{Z}_2]\{\boldsymbol{\varepsilon}_{br}\} + \{\boldsymbol{\varepsilon}_{bnr}\},$$
$$\{\boldsymbol{\varepsilon}_b\}_t = \{\boldsymbol{\varepsilon}_{bt}\} + [\mathbf{Z}_3]\{\boldsymbol{\varepsilon}_{br}\} + \{\boldsymbol{\varepsilon}_{bnr}\}$$

and $\{\boldsymbol{\varepsilon}_b\}_p = \{\boldsymbol{\varepsilon}_{bt}\} + [\mathbf{Z}_4]\{\boldsymbol{\varepsilon}_{br}\} + \{\boldsymbol{\varepsilon}_{bnr}\}$ (8)

Similarly, the strain vectors $\{\boldsymbol{\varepsilon}_s\}_c, \{\boldsymbol{\varepsilon}_s\}_b, \{\boldsymbol{\varepsilon}_s\}_t, \{\boldsymbol{\varepsilon}_s\}_v$ and $\{\boldsymbol{\varepsilon}_s\}_p$ defining the state of transverse shear strains at any point in the core, the bottom layer, the top layer, the viscoelastic layer and the active constraining layer, respectively, can be expressed as:

$\{\boldsymbol{\varepsilon}_s\}_c = \{\boldsymbol{\varepsilon}_{st}\} + [\mathbf{Z}_5]\{\boldsymbol{\varepsilon}_{sr}\} + \{\boldsymbol{\varepsilon}_{snr}\}$,
$\{\boldsymbol{\varepsilon}_s\}_b = \{\boldsymbol{\varepsilon}_{st}\} + [\mathbf{Z}_6]\{\boldsymbol{\varepsilon}_{sr}\} + \{\boldsymbol{\varepsilon}_{snr}\}$,
$\{\boldsymbol{\varepsilon}_s\}_t = \{\boldsymbol{\varepsilon}_{st}\} + [\mathbf{Z}_7]\{\boldsymbol{\varepsilon}_{sr}\} + \{\boldsymbol{\varepsilon}_{snr}\}$,
$\{\boldsymbol{\varepsilon}_s\}_v = \{\boldsymbol{\varepsilon}_{st}\} + [\mathbf{Z}_8]\{\boldsymbol{\varepsilon}_{sr}\} + \{\boldsymbol{\varepsilon}_{snr}\}$ and
$\{\boldsymbol{\varepsilon}_s\}_p = \{\boldsymbol{\varepsilon}_{st}\} + [\mathbf{Z}_9]\{\boldsymbol{\varepsilon}_{sr}\} + \{\boldsymbol{\varepsilon}_{snr}\}$ (9)

The various matrices appearing in the above equations have been defined in the Appendix, while the generalized strain vectors appearing in Eqs. (8) and (9) are given by

$$\{\boldsymbol{\varepsilon}_{bt}\} = \left[\frac{\partial u_0}{\partial x} \quad \frac{\partial v_0}{\partial y} \quad \frac{\partial v_0}{\partial y} + \frac{\partial v_0}{\partial x} \quad 0\right]^T \text{ and}$$

$$\{\boldsymbol{\varepsilon}_{st}\} = \left[\frac{\partial w_0}{\partial x} \quad \frac{\partial w_0}{\partial y}\right]^T \tag{10}$$

$$\{\boldsymbol{\varepsilon}_{br}\} = \left[\frac{\partial \theta_x}{\partial x} \quad \frac{\partial \theta_y}{\partial y} \quad \frac{\partial \theta_y}{\partial x} + \frac{\partial \theta_x}{\partial y} \quad \theta_z \quad \frac{\partial \phi_x}{\partial x} \quad \frac{\partial \phi_y}{\partial y} \quad \frac{\partial \phi_y}{\partial x} + \frac{\partial \phi_x}{\partial y} \quad \phi_z \quad \frac{\partial \alpha_x}{\partial x} \quad \frac{\partial \alpha_y}{\partial y} \quad \frac{\partial \alpha_y}{\partial x} + \frac{\partial \alpha_x}{\partial y} \quad \alpha_z \quad \frac{\partial \beta_x}{\partial x} \quad \frac{\partial \beta_y}{\partial y} \quad \frac{\partial \beta_y}{\partial x} + \frac{\partial \beta_x}{\partial y} \quad \beta_z \quad \frac{\partial \gamma_x}{\partial x} \quad \frac{\partial \gamma_y}{\partial y} \quad \frac{\partial \gamma_y}{\partial x} + \frac{\partial \gamma_x}{\partial y} \quad \gamma_z\right]^T \tag{11}$$

$$\{\boldsymbol{\varepsilon}_{sr}\} = \left[\theta_x \ \theta_y \ \phi_x \ \phi_y \ \alpha_x \ \alpha_y \ \beta_x \ \beta_y \ \gamma_x \ \gamma_y \ \frac{\partial \theta_z}{\partial x} \ \frac{\partial \theta_z}{\partial y} \ \frac{\partial \phi_z}{\partial x} \ \frac{\partial \phi_z}{\partial y} \ \frac{\partial \alpha_z}{\partial x} \ \frac{\partial \alpha_z}{\partial y} \ \frac{\partial \beta_z}{\partial x} \ \frac{\partial \beta_z}{\partial y} \ \frac{\partial \gamma_z}{\partial x} \ \frac{\partial \gamma_z}{\partial y}\right]^T \tag{12}$$

$$\{\boldsymbol{\varepsilon}_{bnr}\} = \frac{1}{2}\left[\left(\frac{\partial w_0}{\partial x}\right)^2 \ \left(\frac{\partial w_0}{\partial y}\right)^2 \ 0 \ 2\frac{\partial w_0}{\partial x}\frac{\partial w_0}{\partial y}\right]^T \text{ and}$$

$$\{\boldsymbol{\varepsilon}_{snr}\} = \frac{1}{2}\left[2\frac{\partial u_0}{\partial x}\frac{\partial w_0}{\partial z} \ \ 2\frac{\partial v_0}{\partial y}\frac{\partial w_0}{\partial z}\right]^T \tag{13}$$

In consistent with the state of strains given by Eq. (7), the state of stresses at any point in the overall plate is described by the two stress vectors as follows:

$$\{\boldsymbol{\sigma}_b\} = \left[\sigma_x \ \sigma_y \ \sigma_{xy} \ \sigma_z\right]^T \text{ and } \{\boldsymbol{\sigma}_s\} = \left[\sigma_{xz} \ \sigma_{yz}\right]^T \tag{14}$$

where, $\sigma_x, \sigma_y, \sigma_z$ are the normal stresses along x, y and z directions, respectively; σ_{xy} is the in-plane shear stress; σ_{xz} , σ_{yz} are the transverse shear stresses.

The top and the bottom facings of the sandwich plate are considered to be isotropic FGMs made of two homogenous constituents namely a ceramic and a metal. The two constituent materials are assumed to be isotropic and linearly elastic whose volume fractions vary across the thickness direction only. The effective material properties of each layer, like the young's modulus, the Poisson's ration and the density at any point can be expressed as,

$$E_{fg}^k(z) = E_m + (E_c - E_m)V^k, \ v_{fg}^k(z) = v_m + (v_c - v_m)V^k$$
and $\rho_{fg}^k(z) = \rho_m + (\rho_c - \rho_m)V^k$ (15)

where the volume fraction V^k of the k^{th} layer (k=1, 2, 3) of the **FG** sandwich plate are given by

$$V^1 = \left(\frac{z - h_1}{h_2 - h_1}\right)^r, \ z \in [h_1, h_2]$$

$$V^2 = 1, z \in [h_2, h_3] \tag{16}$$

$$V^3 = \left(\frac{z - h_3}{h_3 - h_4}\right)^r, \ z \in [h_3, h_2]$$

while the subscripts m and c represent the metallic and ceramic phases of the FGM, respectively. If the values of the superscript k are 1, 2 and 3, it represents the bottom layer, the core and the top layer of the plate, respectively. Also, the variable r is the power-law index (greater than or equal to zero) which determines the material variation profile through the thickness of the top and the bottom facings. The core is independent of 'r' making it fully ceramic layer. The constitutive relation for the materials of the different layers of the FG sandwich plate are given by

$$\{\boldsymbol{\sigma}_b\}_{fg}^k = [\mathbf{C}_b]_{fg}^k\left(\{\boldsymbol{\varepsilon}_b\}_{fg}^k - \{\alpha_b\}_{fg}^k \Delta T\right) \text{ and}$$

$$\{\boldsymbol{\sigma}_s\}_{fg}^k = [\mathbf{C}_s]_{fg}^k\{\boldsymbol{\varepsilon}_s\}_{fg}^k \tag{17}$$

where $[\mathbf{C}_b]_{fg}^k = [\mathbf{C}_b]_m\left[1 + \left(\frac{E_c}{E_m} - 1\right)V^k\right]$,

$$[\mathbf{C}_s]_{fg}^k = [\mathbf{C}_s]_m\left[1 + \left(\frac{E_c}{E_m} - 1\right)V^k\right],$$

$$\{\alpha_b\}_{fg}^k = [{\alpha_x}^b(z) \ \ {\alpha_x}^b(z) \ \ 0 \ \ 0]^T, \Delta T = T(z) - T_0 \tag{18}$$

$$[\mathbf{C}_b]_m = \frac{E_m}{(1+v)(1+2v)}\begin{bmatrix} (1-v) & v & 0 & v \\ v & (1-v) & 0 & v \\ 0 & 0 & (1-2v) & 0 \\ v & v & 0 & (1-v) \end{bmatrix}$$

and

$$[\mathbf{C}_s]_m = \frac{E_m}{2(1+v)}\begin{bmatrix} 1 & 0 \\ 0 & 1 \end{bmatrix} \tag{19}$$

Wherein, ${\alpha_x}^b(z)$ and ${\alpha_x}^b(z)$ are the coefficients of thermal expansion of the bottom FG layer in x and y directions, respectively . Also, ${\alpha_x}^b(z) = {\alpha_x}^b(z) = \alpha_{FG}$. In Eq. 18, $T(z)$ is the temperature at any point in the FG bottom layer which can be determined by the steady-state one dimensional heat conduction equation [37-39] satisfying the boundary conditions $T = T_c$ at the bottom surface of the substrate plate while $T = T_0$ at the interface between the bottom FG layer and the core is given by

$$\frac{d}{dz}\left(K_{fg}\frac{dT}{dz}\right) = 0 \tag{20}$$

Where, K_{fg} is the thermal conductivity of the FG bottom isotropic layer. The solution of Eq. (20) can be readily obtained from [37, 39]. The core may be composed of HEREX honeycomb material. For the purpose of modeling the flexible honeycomb core, the core is assumed to be an equivalent homogeneous solid continuum [2, 9] whose corresponding constitutive relations are given by

$$\{\boldsymbol{\sigma}_b^c\}_{core} = [\mathbf{C}_b^c]\{\boldsymbol{\varepsilon}_b\} \text{ and } \{\boldsymbol{\sigma}_s^c\}_{core} = [\mathbf{C}_s^c]\{\boldsymbol{\varepsilon}_s\} \tag{21}$$

where $[\mathbf{C}_b^c] = \begin{bmatrix} C_{11}^c & C_{12}^c & C_{16}^c & C_{13}^c \\ C_{21}^c & C_{22}^c & C_{26}^c & C_{23}^c \\ C_{16}^c & C_{26}^c & C_{66}^c & C_{36}^c \\ C_{31}^c & C_{32}^c & C_{36}^c & C_{33}^c \end{bmatrix}$ and $[\mathbf{C}_s^c] = \begin{bmatrix} C_{55}^c & C_{45}^c \\ C_{45}^c & C_{44}^c \end{bmatrix}$

The material of the viscoelastic layer is assumed to be linearly viscoelastic and isotropic. The present study is concerned with the analysis of FG sandwich plates undergoing ACLD in the time domain. Hence, the viscoelastic material is modeled by the Golla-Hughes-McTavish (GHM) method. In time domain, the constitutive relation for the viscoelastic material is represented by the following Stieltjes integral form [49].

$$\{\boldsymbol{\sigma}_s\}_V = \int_0^t G(t-\tau)\frac{\partial\{\boldsymbol{\varepsilon}_s\}_V}{\partial\tau}d\tau \tag{22}$$

where $G(t)$ is the relaxation function of the viscoelastic material.

The constraining 1-3 PZC layer is considered to be subjected to the electric field E_z along the $z-$ direction only. Thus the constitutive relations for the constraining 1-3 PZC layer of the ACLD treatment are given by [31]

$$\{\boldsymbol{\sigma}_b\}_p = [\mathbf{C}_b]_p\{\boldsymbol{\varepsilon}_b\}_p + [\mathbf{C}_{bs}]_p\{\boldsymbol{\varepsilon}_s\}_p - \{\mathbf{e}_b\}E_z \ ,$$

$$\{\boldsymbol{\sigma}_s\}_p = \{\boldsymbol{\varepsilon}_b\}_p + [\mathbf{C}_s]_p\{\boldsymbol{\varepsilon}_s\}_p - \{\mathbf{e}_s\}E_z \text{ and}$$

$$D_z = \{\mathbf{e}_b\}^T\{\boldsymbol{\varepsilon}_b\}_p + \{\mathbf{e}_s\}^T\{\boldsymbol{\varepsilon}_s\}_p + \epsilon_{33}E_z \tag{23}$$

Here, D_z represents the electric displacement along the $z-$direction and ϵ_{33} is the dielectric constant. The forms of the transformed elastic coefficient matrices $[\mathbf{C}_\mathrm{b}]_\mathrm{p}$ and $[\mathbf{C}_\mathrm{s}]_\mathrm{p}$ are similar to those of $[\mathbf{C}_\mathrm{b}^c]$ and $[\mathbf{C}_\mathrm{s}^c]$, respectively. It may be noted from the above form of constitutive relations that the transverse shear strains are coupled with the in-plane stresses due to the orientation of piezoelectric fibers in the vertical $xz-$ or $yz-$plane and the corresponding elastic coupling constant matrix $[\mathbf{C}_{bs}]_p$ is given by

$$[\mathbf{C}_\mathrm{bs}]_\mathrm{p}=\begin{bmatrix} C_{15} & 0 \\ C_{25} & 0 \\ 0 & C_{46} \\ C_{35} & 0 \end{bmatrix} \text{ or } [\mathbf{C}_\mathrm{bs}]_\mathrm{p}=\begin{bmatrix} 0 & C_{14} \\ 0 & C_{24} \\ C_{56} & 0 \\ 0 & C_{34} \end{bmatrix} \tag{24}$$

according as the piezoelectric fibers are coplanar with the vertical $xz-$ or $yz-$plane. Note that if the fibers are coplanar with the $xz-$ and the $yz-$ planes, this coupling matrix becomes a null matrix. Also, the piezoelectric constant matrices $\{\mathbf{e}_b\}$ and $\{\mathbf{e}_s\}$ appearing in Eq. (23) contain the following transformed effective piezoelectric coefficients of the 1-3 PZC:

$$\{\mathbf{e}_b\} = \{\bar{e}_{31}\ \bar{e}_{32}\ \bar{e}_{36}\ \bar{e}_{33}\}^T \text{ and } \{\mathbf{e}_s\} = \{\bar{e}_{35}\ \bar{e}_{34}\}^T \tag{25}$$

The total potential energy T_p and the total kinetic energy T_k of the overall plate /ACLD system are given by

$$T_p = \frac{1}{2}\Big\{\int_\Omega\big(\{\boldsymbol{\varepsilon}_b\}_c{}^T\{\boldsymbol{\sigma}_b\}_c + \{\boldsymbol{\varepsilon}_s\}_c{}^T\{\boldsymbol{\sigma}_s\}_c\big)\,\mathrm{d}\Omega + \int_\Omega\Big(\{\boldsymbol{\varepsilon}_b\}_{fg}^1{}^T\{\boldsymbol{\sigma}_b\}_{fg}^1 + \{\boldsymbol{\varepsilon}_s\}_{fg}^1{}^T\{\boldsymbol{\sigma}_s\}_{fg}^1\Big) + \int_\Omega\Big(\{\boldsymbol{\varepsilon}_b\}_{fg}^3{}^T\{\boldsymbol{\sigma}_b\}_{fg}^3 + \{\boldsymbol{\varepsilon}_s\}_{fg}^3{}^T\{\boldsymbol{\sigma}_s\}_{fg}^3\Big) + \int_\Omega\big(\{\boldsymbol{\varepsilon}_s\}_v{}^T\{\boldsymbol{\sigma}_s\}_v\big)\,\mathrm{d}\Omega + \int_\Omega\big(\{\boldsymbol{\varepsilon}_b\}_p{}^T\{\boldsymbol{\sigma}_b\}_p + \{\boldsymbol{\varepsilon}_s\}_p{}^T\{\boldsymbol{\sigma}_s\}_p\big)\,\mathrm{d}\Omega - \int_\Omega D_z E_z\,\mathrm{d}\Omega\Big\} - \int_A\{\mathbf{d}\}^T\{\mathbf{f}\}\mathrm{dA} \tag{26}$$

$$T_k = \frac{1}{2}\Big\{\int_\Omega\rho_c\big(\dot{u}^2+\dot{v}^2+\dot{w}^2\big)\,\mathrm{d}\Omega + \int_\Omega\rho_v\big(\dot{u}_v{}^2+\dot{v}_v{}^2+\dot{w}_v{}^2\big)\,\mathrm{d}\Omega + \int_\Omega\rho_p\big(\dot{u}_p{}^2+\dot{v}_p{}^2+\dot{w}_p{}^2\big)\,\mathrm{d}\Omega + \int_\Omega\rho_{fg}^1\big(\dot{u}^2+\dot{v}^2+\dot{w}^2\big)\,\mathrm{d}\Omega + \int_\Omega\rho_{fg}^3\big(\dot{u}^2+\dot{v}^2+\dot{w}^2\big)\,\mathrm{d}\Omega\Big\} \tag{27}$$

in which ρ_c, ρ_v and ρ_p are the mass densities of the core, the viscoelastic layer and the 1-3 PZC layers, respectively; ρ_{fg}^1 and ρ_{fg}^3 are the densities any point in the bottom and the top layers, respectively; $\{\mathbf{f}\} = [0 \quad 0 \quad P]^T$ is the externally applied surface traction acting over a surface area A with P being the transverse distributed pulse loading over the surface and Ω represents the volume of the concerned layer. Since, the thickness of the plate is very small compared to the lateral dimensions of the plate, the rotary inertia of the overall plate is neglected in estimating the total kinetic energy.

FINITE ELEMENT MODEL OF FG SANDWICH PLATE INTEGRATED WITH ACLD PATCHES

Eight noded isoparametric serendipity elements have been used to discretize the smart FG sandwich plate. Following Eq. (6), the generalized displacement vectors $\{\mathbf{d}_{ti}\}$ and $\{\mathbf{d}_{ri}\}$ associated with the i$^{\text{th}}$ (i=1, 2, 3,…8) node of the element can be written as

$$\{\mathbf{d}_{ti}\} = [u_{0i}\ \ v_{0i}\ \ w_{0i}]^T \text{ and}$$

$$\{\mathbf{d}_{ri}\} = \big[\theta_{xi}\ \ \theta_{yi}\ \ \theta_{zi}\ \ \phi_{xi}\ \ \phi_{yi}\ \ \phi_{zi}\ \ \alpha_{xi}\ \ \alpha_{yi}\ \ \alpha_{zi}\ \ \beta_{xi}\ \ \beta_{yi}\ \ \beta_{zi}\ \ \gamma_{xi}\ \ \gamma_{yi}\ \ \gamma_{zi}\big]^T \tag{28}$$

Thus the elemental displacement vectors at any point within the element can be can be expressed in terms of the nodal generalized displacement vectors $\{\mathbf{d}_\mathbf{t}^\mathbf{e}\}$ and $\{\mathbf{d}_\mathbf{r}^\mathbf{e}\}$ as follows:

$$\{\mathbf{d}_t\} = [\mathbf{N}_t]\{\mathbf{d}_t^e\} \text{ and } \{\mathbf{d}_r\} = [\mathbf{N}_r]\{\mathbf{d}_r^e\} \tag{29}$$

in which $[\mathbf{N}_t] = [N_{t1}\ \ N_{t2}\ ....\ \ N_{t8}]^T$,

$[\mathbf{N}_r] = [N_{r1}\ \ N_{r2}\ ....\ \ N_{r8}]^T$, $N_{ti} = n_i I_t$, $N_{ri} = n_i I_r$

$\{\mathbf{d}_t^e\} = [\{\mathbf{d}_{t1}^e\}^T\ \ \{\mathbf{d}_{t2}^e\}^T\ \ ...\ \ \{\mathbf{d}_{t8}^e\}^T]^T$ and

$\{\mathbf{d}_r^e\} = [\{\mathbf{d}_{r1}^e\}^T\ \ \{\mathbf{d}_{r2}^e\}^T\ \ ...\ \ \{\mathbf{d}_{r8}^e\}^T]^T$ (30)

while I_t and I_r are the (3 x 3) and the (15 x 15) identity matrices, respectively and n_i is the shape function in natural coordinates associated with the i$^{\text{th}}$ node. Making use of the relation given by Eqs. (9)-(13), (27) and (28), the strain vectors at any point within the element can be expressed in terms of the nodal displacement vectors as follows:

$$\{\boldsymbol{\varepsilon}_b\}_c = [\mathbf{B}_{tb}]\{\mathbf{d}_t^e\} + [\mathbf{Z}_1][\mathbf{B}_{rb}]\{\mathbf{d}_r^e\} + \frac{1}{2}[\mathbf{B}_1][\mathbf{B}_2]\{\mathbf{d}_t^e\},$$

$$\{\boldsymbol{\varepsilon}_b\}_b = [\mathbf{B}_{tb}]\{\mathbf{d}_t^e\} + [\mathbf{Z}_2][\mathbf{B}_{rb}]\{\mathbf{d}_r^e\} + \frac{1}{2}[\mathbf{B}_1][\mathbf{B}_2]\{\mathbf{d}_t^e\}$$

$$\{\boldsymbol{\varepsilon}_b\}_t = [\mathbf{B}_{tb}]\{\mathbf{d}_t^e\} + [\mathbf{Z}_3][\mathbf{B}_{rb}]\{\mathbf{d}_r^e\} + \frac{1}{2}[\mathbf{B}_1][\mathbf{B}_2]\{\mathbf{d}_t^e\},$$

$$\{\boldsymbol{\varepsilon}_b\}_p = [\mathbf{B}_{tb}]\{\mathbf{d}_t^e\} + [\mathbf{Z}_4][\mathbf{B}_{rb}]\{\mathbf{d}_r^e\} + \frac{1}{2}[\mathbf{B}_1][\mathbf{B}_2]\{\mathbf{d}_t^e\} \ ,$$

$$\{\boldsymbol{\varepsilon}_s\}_c = [\mathbf{B}_{ts}]\{\mathbf{d}_t^e\} + [\mathbf{Z}_5][\mathbf{B}_{rs}]\{\mathbf{d}_r^e\},$$

$$\{\boldsymbol{\varepsilon}_s\}_b = [\mathbf{B}_{ts}]\{\mathbf{d}_t^e\} + [\mathbf{Z}_6][\mathbf{B}_{rs}]\{\mathbf{d}_r^e\}$$

$$\{\boldsymbol{\varepsilon}_s\}_t = [\mathbf{B}_{ts}]\{\mathbf{d}_t^e\} + [\mathbf{Z}_7][\mathbf{B}_{rs}]\{\mathbf{d}_r^e\},$$

$$\{\boldsymbol{\varepsilon}_s\}_v = [\mathbf{B}_{ts}]\{\mathbf{d}_t^e\} + [\mathbf{Z}_8][\mathbf{B}_{rs}]\{\mathbf{d}_r^e\},$$

$$\{\boldsymbol{\varepsilon}_s\}_p = [\mathbf{B}_{ts}]\{\mathbf{d}_t^e\} + [\mathbf{Z}_9][\mathbf{B}_{rs}]\{\mathbf{d}_r^e\} \tag{31}$$

in which the nodal strain displacement matrices $[\mathbf{B}_{tb}]$, $[\mathbf{B}_{rb}]$, $[\mathbf{B}_{ts}]$, $[\mathbf{B}_{rs}]$, $[\mathbf{B}_1]$ and $[\mathbf{B}_2]$ are given by

$[\mathbf{B}_{tb}] = [B_{tb1}\ \ B_{tb2}\ ...\ \ B_{tb8}]$, $[\mathbf{B}_{rb}] = [B_{rb1}\ \ B_{rb2}\ ...\ \ B_{rb8}]$,

$$[\mathbf{B}_{ts}] = [B_{ts1}\ \ B_{ts2}\ \ldots\ \ B_{ts8}],\ \ [\mathbf{B}_{rs}] = [B_{rs1}\ \ B_{rs2}\ \ldots\ \ B_{rs8}]$$

$$[\mathbf{B}_1] = \begin{bmatrix} \frac{\partial w_0}{\partial x} & 0 & \frac{\partial w_0}{\partial y} & 0 \\ 0 & \frac{\partial w_0}{\partial y} & \frac{\partial w_0}{\partial x} & 0 \end{bmatrix}^T, [\mathbf{B}_2] = [B_{21} \quad B_{22} \quad \ldots \quad B_{28}] \tag{32}$$

The submatrices of $[\mathrm{B}_{tb}]$,$[\mathrm{B}_{rb}]$, $[\mathrm{B}_{ts}]$, $[\mathrm{B}_{2i}]$ and $[\mathrm{B}_{rs}]$ shown in Eq. (30) have been explicitly presented in the Appendix.

Finally, substituting Eqs. (15)- (25) and (31) into Eq. (26) and recognizing that $E_z = -V/h_p$ with V being the applied voltage across the thickness of the piezoelectric layer, the total potential energy T_p^e of a typical element integrated with the ACLD treatment can be expressed as

$$\begin{aligned} T_p^e = \frac{1}{2}\,[\{\mathbf{d}_t^e\}^T\,[\mathbf{K}_{tt}^e]\,\{\mathbf{d}_t^e\} + \{\mathbf{d}_t^e\}^T[\mathbf{K}_{tr}^e]\{\mathbf{d}_r^e\} \\ + \{\mathbf{d}_r^e\}^T[\mathbf{K}_{rt}^e]\,\{\mathbf{d}_t^e\} + \{\mathbf{d}_r^e\}^T[\mathbf{K}_{rr}^e]\{\mathbf{d}_r^e\} \\ + \{\mathbf{d}_t^e\}^T[\mathbf{K}_{tsv}^e]\int_0^t G(t-\tau)\frac{\partial}{\partial\tau}\{\mathbf{d}_t^e\}\mathrm{d}\tau \\ + \{\mathbf{d}_t^e\}^T[\mathbf{K}_{trsv}^e]\int_0^t G(t-\tau)\frac{\partial}{\partial\tau}\{\mathbf{d}_r^e\}\mathrm{d}\tau \\ + \{\mathbf{d}_r^e\}^T[\mathbf{K}_{trsv}^e]^T\int_0^t G(t-\tau)\frac{\partial}{\partial\tau}\{\mathbf{d}_t^e\}\mathrm{d}\tau \\ + \{\mathbf{d}_r^e\}^T\,[\mathbf{K}_{rrsv}^e]\int_0^t G(t-\tau)\frac{\partial}{\partial\tau}\{\mathbf{d}_r^e\}\mathrm{d}\tau \\ -2\{\mathbf{d}_t^e\}^T\{\mathbf{F}_{tp}^e\}V - 2\{\mathbf{d}_t^e\}^T\{\mathbf{F}_{tpn}^e\}V - 2\{\mathbf{d}_r^e\}^T\{\mathbf{F}_{rp}^e\}V - \\ \frac{\bar{\epsilon}_{33}V^2}{h_p} - 2\{\mathbf{d}_t^e\}^T\{\mathbf{F}^e\} - \{\mathbf{d}_t^e\}^T\{\mathbf{F}_{Tb}^e\} - \{\mathbf{d}_t^e\}^T\{\mathbf{F}_{Tr}^e\} \end{aligned} \tag{33}$$

The elemental stiffness matrices ($[\mathbf{K}_{tt}^e]$, $[\mathbf{K}_{tr}^e]$, $[\mathbf{K}_{rt}^e]$, $[\mathbf{K}_{rr}^e]$, $[\mathbf{K}_{tsv}^e]$, $[\mathbf{K}_{trsv}^e]$ and $[\mathbf{K}_{rrsv}^e]$) the elemental electro-elastic coupling matrices ($\{\mathbf{F}_{tp}^e\}$, $\{\mathbf{F}_{tpn}^e\}$ and $\{\mathbf{F}_{rp}^e\}$), $\{\mathbf{F}_{Tb}^e\}$, $\{\mathbf{F}_{Tr}^e\}$ and the elemental load vector $\{\mathbf{F}^e\}$ appearing in Eq. (31) are derived as follows:

$$\begin{aligned} &[\mathbf{K}_{tt}^e] = [\mathbf{K}_{tb}^e] + [\mathbf{K}_{ts}^e] + [\mathbf{K}_{tnb}^e]\ , \\ &[\mathbf{K}_{tr}^e] = [\mathbf{K}_{trb}^e] + [\mathbf{K}_{trs}^e] + [\mathbf{K}_{trbn}^e]\ , \\ &[\mathbf{K}_{rt}^e] = [\mathbf{K}_{trb}^e]^T + [\mathbf{K}_{trs}^e]^T + \tfrac{1}{2}[\mathbf{K}_{trbn}^e]^T\ , \\ &[\mathbf{K}_{rr}^e] = [\mathbf{K}_{rrb}^e] + [\mathbf{K}_{rrs}^e]\ , \\ &\{\mathbf{F}_{tp}^e\} = \{\mathbf{F}_{tb}^e\} + \{\boldsymbol{F}_{ts}^e\} + \{\mathbf{F}_{tpn}^e\}\ , \\ &\{\mathbf{F}_{rp}^e\} = \{\mathbf{F}_{rb}^e\} + \{\mathbf{F}_{rs}^e\} \end{aligned} \tag{34}$$

where

$$\begin{aligned} &[\mathbf{K}_{tb}^e] = \\ &\int_0^{a_e}\int_0^{b_e}[\mathbf{B}_{tb}]^T\left(\left[\mathbf{D}_{tb}^b\right] + [\mathbf{D}_{tb}^c] + [\mathbf{D}_{tb}^t] + \left[\mathbf{D}_{tb}^p\right]\right)[\mathbf{B}_{tb}]\,\mathrm{dx\,dy} + \\ &\int_0^{a_e}\int_0^{b_e}[\mathbf{B}_{tb}]^T\left[\mathbf{D}_{tbs}^p\right][\mathbf{B}_{ts}]\mathrm{dx\,dy}\,, \end{aligned}$$

$$\begin{aligned} [\mathbf{K}_{trb}^e] = \int_0^{a_e}\int_0^{b_e}[\mathbf{B}_{tb}]^T\left(\left[\mathbf{D}_{trb}^b\right]\left[\mathbf{B}_{rb}{}^b\right] + [\mathbf{D}_{trb}^c][\mathbf{B}_{rb}{}^c]\right. \\ + [\mathbf{D}_{trb}^t]\left[\mathbf{B}_{rb}{}^t\right] + \left[\mathbf{D}_{trb}^p\right][\mathbf{B}_{rb}{}^v] \\ \left. + \left[\mathbf{D}_{trbs}^p\right][\mathbf{B}_{rs}{}^p]\right)\mathrm{dx\,dy}\,, \end{aligned}$$

$$\begin{aligned} [\mathbf{K}_{rtb}^e] = \int_0^{a_e}\int_0^{b_e}\left(\left[\mathbf{B}_{rb}{}^b\right]^T\left[\mathbf{D}_{trb}^b\right]^T + [\mathbf{B}_{rb}{}^c]^T[\mathbf{D}_{trb}^c]^T\right. \\ + \left[\mathbf{B}_{rb}{}^t\right]^T[\mathbf{D}_{trb}^t]^T \\ \left. + [\mathbf{B}_{rb}{}^p]^T\left[\mathbf{D}_{trb}^p\right]^T\right)[\mathbf{B}_{tb}]\,\mathrm{dx\,dy} \\ + \int_0^{a_e}\int_0^{b_e}[\mathbf{B}_{rb}{}^p]^T\left[\mathbf{D}_{rtbs}^p\right]^T[\mathbf{B}_{ts}]\mathrm{dx\,dy}\,, \end{aligned}$$

$$\begin{aligned} [\mathbf{K}_{rrb}^e] = \int_0^{a_e}\int_0^{b_e}\left(\left[\mathbf{B}_{rb}{}^b\right]^T\left[\mathbf{D}_{rrb}^b\right]\left[\mathbf{B}_{rb}{}^b\right]\right. \\ + [\mathbf{B}_{rb}{}^c]^T[\mathbf{D}_{rrb}^c][\mathbf{B}_{rb}{}^c] \\ + \left[\mathbf{B}_{rb}{}^t\right]^T[\mathbf{D}_{rrb}^t]\left[\mathbf{B}_{rb}{}^t\right] \\ + [\mathbf{B}_{rb}{}^p]^T\left[\mathbf{D}_{rrb}^p\right][\mathbf{B}_{rb}{}^p] \\ \left. + [\mathbf{B}_{rb}{}^p]^T\left[\mathbf{D}_{rrbs}^p\right][\mathbf{B}_{rs}{}^p]\right)\mathrm{dx\,dy}, \end{aligned}$$

$$\begin{aligned} [\mathbf{K}_{tbn}^e] = \int_0^{a_e}\int_0^{b_e}\left\{[\mathbf{B}_{tb}]^T\left(\left[\mathbf{D}_{tb}^b\right] + [\mathbf{D}_{tb}^c] + [\mathbf{D}_{tb}^t]\right.\right. \\ \left. + \left[\mathbf{D}_{tb}^p\right]\right)\frac{1}{2}[\mathbf{B}_1][\mathbf{B}_2] \\ + [\mathbf{B}_{ts}]^T\left[\mathbf{D}_{tbs}^p\right]^T\frac{1}{2}[\mathbf{B}_1][\mathbf{B}_2] \\ + [\mathbf{B}_2]^T[\mathbf{B}_1]^T\left(\left[\mathbf{D}_{tb}^b\right] + [\mathbf{D}_{tb}^c] + [\mathbf{D}_{tb}^t]\right. \\ \left. + \left[\mathbf{D}_{tb}^p\right])[\mathbf{B}_{tb}] + [\mathbf{B}_2]^T[\mathbf{B}_1]^T\left[\mathbf{D}_{tbs}^p\right][\mathbf{B}_{ts}] \\ + [\mathbf{B}_2]^T[\mathbf{B}_1]^T\left(\left[\mathbf{D}_{tb}^b\right] + [\mathbf{D}_{tb}^c] + [\mathbf{D}_{tb}^t]\right. \\ \left.\left. + \left[\mathbf{D}_{tb}^p\right])\frac{1}{2}[\mathbf{B}_1][\mathbf{B}_2]\right\}\mathrm{dx\,dy}\,, \end{aligned}$$

$$\begin{aligned} [\mathbf{K}_{trbn}^e] = \int_0^{a_e}\int_0^{b_e}\left([\mathbf{B}_2]^T[\mathbf{B}_1]^T[\mathbf{D}_{tr}^b][\mathbf{B}_{rb}]\right. \\ + [\mathbf{B}_2]^T[\mathbf{B}_1]^T\left[\mathbf{D}_{trb}^b\right][\mathbf{B}_{rb}^c] \\ + [\mathbf{B}_2]^T[\mathbf{B}_1]^T\left[\mathbf{D}_{trb}^b\right][\mathbf{B}_{rb}^t] \\ + [\mathbf{B}_2]^T[\mathbf{B}_1]^T\left[\mathbf{D}_{trb}^p\right]\left[\mathbf{B}_{rb}^p\right] \\ \left. + [\mathbf{B}_2]^T[\mathbf{B}_1]^T\left[\mathbf{D}_{trbs}^p\right]\left[\mathbf{B}_{rs}^p\right]\right)\mathrm{dx\,dy}\,, \end{aligned}$$

$$[\mathbf{K}_{rtbn}^e] = \tfrac{1}{2}[\mathbf{K}_{rtbn}^e]^T,\ \{\mathbf{F}_{tb}^e\} = \int_0^{a_e}\int_0^{b_e}[\mathbf{B}_{tb}]^T\{\mathbf{D}_{tp}^b\}\,\mathrm{dx\,dy}$$

$$,\{\mathbf{F}_{rb}^e\}_p = \int_0^{a_e}\int_0^{b_e}[\mathbf{B}_{tb}{}^p]^T\{\mathbf{D}_{rb}^p\}\,\mathrm{dx\,dy}\,,$$

$$\{\mathbf{F}_{tb}^e\} = \int_0^{a_e}\int_0^{b_e}[\mathbf{B}_2]^T[\mathbf{B}_1]^T\{\mathbf{D}_{tp}\}\,\mathrm{dx\,dy}\,.$$

$$\begin{aligned} &\{\mathbf{F}_{Tb}^e\} = \\ &\int_0^{a_e}\int_0^{b_e}[\mathbf{B}_{tb}]^T[\mathbf{D}_{tbt}]\,\mathrm{dx\,dy} + \int_0^{a_e}\int_0^{b_e}\tfrac{1}{2}[\mathbf{B}_2]^T[\mathbf{B}_1]^T[\mathbf{D}_{tbt}]\,\mathrm{dx\,dy} \\ &\{\mathbf{F}_{Tr}^e\} = \int_0^{a_e}\int_0^{b_e}[\mathbf{B}_{rb}]^T[\mathbf{D}_{rbt}]\,\mathrm{dx\,dy} \end{aligned} \tag{35}$$

and those associated with the transverse shear deformations are

$$\begin{aligned} &[\mathbf{K}_{ts}^e] = \\ &\int_0^{a_e}\int_0^{b_e}[\mathbf{B}_{ts}]^T\left([\mathbf{D}_{ts}^b] + [\mathbf{D}_{ts}^c] + [\mathbf{D}_{ts}^t] + \left[\mathbf{D}_{ts}^p\right]\right)[\mathbf{B}_{ts}]\,\mathrm{dx\,dy} + \\ &\int_0^{a_e}\int_0^{b_e}[\mathbf{B}_{ts}]^T\left[\mathbf{D}_{tbs}^b\right]^T[\mathbf{B}_{tb}]\ \mathrm{dx\,dy}\,, \end{aligned}$$

$$[\mathbf{K}^e_{trs}] = \int_0^{a_e}\int_0^{b_e}\Big\{[\mathbf{B}_{ts}]^T\big([\mathbf{D}^b_{trs}]\big[\mathbf{B}_{rs}{}^b\big] + [\mathbf{D}^c_{trs}][\mathbf{B}_{rs}{}^c] + [\mathbf{D}^t_{trs}]\big[\mathbf{B}_{rs}{}^t\big] + \big[\mathbf{D}^p_{trs}\big][\mathbf{B}_{rs}{}^p]\big) + [\mathbf{B}_{ts}]^T\big[\mathbf{D}^p_{rtbs}\big]^T[\mathbf{B}_{rb}{}^p]\Big\}\,\mathrm{dx\,dy},$$

$$[\mathbf{K}^e_{rts}] = \int_0^{a_e}\int_0^{b_e}\Big\{\Big(\big[\mathbf{B}_{rs}{}^b\big]^T[\mathbf{D}^b_{trs}]^T + [\mathbf{B}_{rs}{}^c][\mathbf{D}^c_{trs}]^T + \big[\mathbf{B}_{rs}{}^t\big]^T[\mathbf{D}^t_{trs}]^T + [\mathbf{B}_{rs}{}^p]^T\big[\mathbf{D}^p_{trs}\big]^T\Big)[\mathbf{B}_{ts}] + [\mathbf{B}_{rs}{}^p]^T\big[\mathbf{D}^p_{trbs}\big]^T[\mathbf{B}_{tb}]\Big\}\,\mathrm{dx\,dy},$$

$$[\mathbf{K}^e_{rrs}] = \int_0^{a_e}\int_0^{b_e}\Big(\big[\mathbf{B}_{rs}{}^b\big]^T[\mathbf{D}^b_{rrs}]\big[\mathbf{B}_{rs}{}^b\big] + [\mathbf{B}_{rs}{}^c]^T[\mathbf{D}^c_{rrs}][\mathbf{B}_{rs}{}^c] + \big[\mathbf{B}_{rs}{}^t\big]^T[\mathbf{D}^t_{rrs}]\big[\mathbf{B}_{rs}{}^t\big] + [\mathbf{B}_{rs}{}^v]^T[\mathbf{D}^v_{rrs}][\mathbf{B}_{rs}{}^v] + [\mathbf{B}_{rs}{}^p]^T\big[\mathbf{D}^p_{rrs}\big][\mathbf{B}_{rs}{}^p]\Big)\,\mathrm{dx\,dy},$$

$$[\mathbf{K}^e_{tsv}] = \int_0^{a_e}\int_0^{b_e}[\mathbf{B}_{ts}]^T[\mathbf{B}_{ts}]h_v\ \mathrm{dx\,dy},$$

$$[\mathbf{K}^e_{trsv}]_s = \int_0^{a_e}\int_0^{b_e}[\mathbf{B}_{rs}]^T[\mathbf{D}^v_{trs}][\,\mathbf{B}^v_{rv}]\ \mathrm{dx\,dy},$$

$$[\mathbf{K}^e_{rrsv}] = \int_0^{a_e}\int_0^{b_e}[\mathbf{B}_{rs}{}^v]^T[\mathbf{D}^v_{rrs}][\mathbf{B}_{rs}{}^v]\ \mathrm{dx\,dy},$$

$$\{\mathbf{F}^e_{ts}\} = \int_0^{a_e}\int_0^{b_e}[\mathbf{B}_{ts}]^T\{\mathbf{D}^s_{tp}\}\,\mathrm{dx\,dy},$$

$$\{\mathbf{F}^e_{rs}\} = \int_0^{a_e}\int_0^{b_e}\big[\mathbf{B}^p_{rs}\big]^T\{\mathbf{D}^s_{rp}\}\,\mathrm{dx\,dy}. \tag{36}$$

where a_e and b_e are the length and the width of the element under consideration and the various rigidity matrices originated in the above elemental stiffness matrices are given in the Appendix. Substituting Eq. (29) into Eq. (27), the expression for the kinetic energy T^e_k of the element can be obtained as

$$T^e_k = \frac{1}{2}\ \{\dot{\mathbf{d}}^e_t\}^T[\mathbf{M}^e]\{\dot{\mathbf{d}}^e_t\} \tag{37}$$

in which

$$[\mathbf{M}^e] = \int_0^{b_e}\int_0^{a_e}\bar{m}\ [\mathbf{N}_t]^T[\mathbf{N}_t]\mathrm{dx\,dy} \quad \text{and}$$

$\bar{m} = 2\rho_c\, h_c + \int_{h_1}^{h_2}\rho^1_{fg}\,\mathrm{dz} + \int_{h_3}^{h_4}\rho^3_{fg}\,\mathrm{dz} + \rho_v\, h_v + \rho_p\, h_p$ for the case of homogenous ceramic core and for flexible HEREX core

$$\bar{m} = 2\rho h_c + \int_{h_1}^{h_2}\rho^1_{fg}\,\mathrm{dz} + \int_{h_3}^{h_4}\rho^3_{fg}\,\mathrm{dz} + \rho_v\, h_v + \rho_p\, h_p \tag{38}$$

Now, applying extended Hamilton's principle for the non-conservative system [34], the following elemental governing equations of motion are obtained:

$$[\mathbf{M}^e]\{\ddot{\mathbf{d}}^e_t\} + [\mathbf{K}^e_{tt}]\{\mathbf{d}^e_t\} + [\mathbf{K}^e_{tr}]\{\mathbf{d}^e_r\} + [\mathbf{K}^e_{tsv}]\int_0^t G(t-\tau)\frac{\partial}{\partial\tau}\{\mathbf{d}^e_t\}\mathrm{d}\tau + [\mathbf{K}^e_{trsv}]\int_0^t G(t-\tau)\frac{\partial}{\partial\tau}\{\mathbf{d}^e_r\}\mathrm{d}\tau = \{\mathbf{F}^e_t\} + \big(\{\mathbf{F}^e_{tp}\} + \{\mathbf{F}^e_{tpn}\}\big)V + \{\mathbf{F}^e_{Tb}\} \tag{39}$$

$$[\mathbf{K}^e_{rt}]\{\mathbf{d}^e_t\} + [\mathbf{K}^e_{rr}]\{\mathbf{d}^e_r\} + [\mathbf{K}^e_{trsv}]^T\int_0^t G(t-\tau)\frac{\partial}{\partial\tau}\{\mathbf{d}^e_t\}\mathrm{d}\tau + [\mathbf{K}^e_{rrsv}]\int_0^t G(t-\tau)\frac{\partial}{\partial\tau}\{\mathbf{d}^e_r\}\mathrm{d}\tau = \{\mathbf{F}^e_{rp}\} + \{\mathbf{F}^e_{Tr}\} \tag{40}$$

It should be noted here that for an element without integrated with the ACLD patch, the matrices $\{\mathbf{F}^e_{tpn}\}$, $\{\mathbf{F}^e_{tp}\}$ and $\{\mathbf{F}^e_{rp}\}$ turn out to be the null matrices. The elemental governing equations are assembled into the global space to obtain the global equations of motion as follows:

$$[\mathbf{M}]\{\ddot{\mathbf{X}}_t\} + [\mathbf{K}_{tt}]\{\mathbf{X}_t\} + [\mathbf{K}_{tr}]\{\mathbf{X}_r\} + [\mathbf{K}_{tsv}]\int_0^t G(t-\tau)\frac{\partial}{\partial\tau}\{\mathbf{X}_t\}\mathrm{d}\tau + [\mathbf{K}_{trsv}]\int_0^t G(t-\tau)\frac{\partial}{\partial\tau}\{\mathbf{X}_r\}\mathrm{d}\tau = \{\mathbf{F}\} + \big(\{\mathbf{F}_{tp}\} + \{\mathbf{F}_{tpn}\}\big)V + \{\mathbf{F}_{Tb}\} \tag{41}$$

$$[\mathbf{K}_{rt}]\{\mathbf{X}_t\} + [\mathbf{K}_{rr}]\{\mathbf{X}_r\} + [\mathbf{K}_{trsv}]^T\int_0^t G(t-\tau)\frac{\partial}{\partial\tau}\{\mathbf{X}_t\}\mathrm{d}\tau + [\mathbf{K}_{rrsv}]\int_0^t G(t-\tau)\frac{\partial}{\partial\tau}\{\mathbf{X}_r\}\mathrm{d}\tau = \{\mathbf{F}_{rp}\}V + \{\mathbf{F}_{Tr}\} \tag{42}$$

where $[\mathbf{M}]$ is the global mass matrix ; $[\mathbf{K}_{tt}]$, $[\mathbf{K}_{tr}]$, $[\mathbf{K}_{rt}]$, $[\mathbf{K}_{rr}]$, $[\mathbf{K}_{tsv}]$, $[\mathbf{K}_{trsv}]$ and $[\mathbf{K}_{rrsv}]$ are the global stiffness matrices, $\{\mathbf{F}_{tp}\}$, $\{\mathbf{F}_{tpn}\}$ and $\{\mathbf{F}_{rp}\}$ are the global electroelastic coupling vectors, $\{\mathbf{X}_t\}$ and $\{\mathbf{X}_r\}$ are the global nodal generalized displacement vectors, $\{\mathbf{F}\}$ is the global nodal mechanical force vector and $\{\mathbf{F}_{Tb}\}$ and $\{\mathbf{F}_{Tr}\}$ are global thermal load vectors. It may be noted that the elements of the matrices $[\mathbf{K}_{tt}]$, $[\mathbf{K}_{tr}]$ and $[\mathbf{K}_{rt}]$ are nonlinear functions of displacements.

After invoking the boundary conditions and taking Laplace transform of Eqs. (39) and (40), the following global equations of motion in Laplace domain are obtained:

$$s^2[\mathbf{M}]\{\tilde{\mathbf{X}}_t\} + \mathcal{L}([\mathbf{K}_{tt}]\{\mathbf{X}_t\} + [\mathbf{K}_{tr}]\{\mathbf{X}_r\}) + [\mathbf{K}_{tsv}]\,s\,\tilde{G}(s)\{\tilde{\mathbf{X}}_t\} + [\mathbf{K}_{trsv}]\,s\,\tilde{G}(s)\{\tilde{\mathbf{X}}_r\} = \{\tilde{\mathbf{F}}_t\} + \mathcal{L}\big(\{\mathbf{F}_{tp}\} + \{\mathbf{F}_{tpn}\}\big)\,\tilde{V} \tag{43}$$

$$\mathcal{L}([\mathbf{K}_{rt}]\{\mathbf{X}_t\}) + [\mathbf{K}_{rr}]\{\tilde{\mathbf{X}}_r\} + [\mathbf{K}_{trsv}]^T\,s\,\tilde{G}(s)\{\tilde{\mathbf{X}}_t\} + [\mathbf{K}_{rrsv}]s\,\tilde{G}(s)\{\tilde{\mathbf{X}}_r\} = \{\mathbf{F}_{rp}\}\,\tilde{V} \tag{44}$$

where $\{\tilde{\mathbf{X}}_t\}$, $\{\tilde{\mathbf{X}}_r\}$, $\{\tilde{\mathbf{F}}\}$ and $\tilde{V}$ are the Laplace transforms of $\{\mathbf{X}_t\}$, $\{\mathbf{X}_r\}$, $\{\mathbf{F}\}$ and V, respectively, $\mathcal{L}$ is the Laplace operator. Also, it may be mentioned that in the Laplace domain, the term $s\tilde{G}(s)$ is referred to as a material modulus function [49].

Employing the GHM method for modeling the viscoelastic material in time domain, the material modulus function can be represented by a series of mini-oscillator terms as follows [49]:

$$s\tilde{G}(s) = G^\infty\left[1 + \sum_{k=1}^N \alpha_k\ \frac{s^2 + 2\hat{\xi}_k\hat{\omega}_k s}{s^2 + 2\hat{\xi}\,\hat{\omega}_k s + \hat{\omega}_k{}^2}\right] \tag{45}$$

where G^∞ corresponds to the equilibrium value of the modulus i.e. the final value of the relaxation function $G(t)$. Each mini-oscillator term is a second-order rational function involving three positive constants α_k, $\hat{\omega}_k$ *and* $\hat{\xi}_k$. These constants govern the shape of the modulus function in the complex s-domain [49]. Now considering a GHM material modulus function with one mini-oscillator term [49] i.e.

$$s\tilde{G}(s) = G^\infty\left[1 + \alpha\ \frac{s^2 + 2\hat{\xi}\hat{\omega}s}{s^2 + 2\hat{\xi}\,\hat{\omega}s + \hat{\omega}^2}\right] \tag{46}$$

the auxiliary dissipation coordinates Z, Z_r are introduced as follows [40]:

$$s\tilde{G}(s)\{\tilde{\mathbf{X}}_t\} = G^\infty\left[(1+\alpha)\{\tilde{\mathbf{X}}_t\} - \alpha\,\{\tilde{\mathbf{Z}}\}\right],\ s\tilde{G}(s)\{\tilde{\mathbf{X}}_r\} = G^\infty\left[(1+\alpha)\{\tilde{\mathbf{X}}_r\} - \alpha\,\{\tilde{\mathbf{Z}}_r\}\right] \tag{47}$$

$$\tilde{Z}(s) = \frac{\hat{\omega}^2}{s^2 + 2\hat{\xi}\,\hat{\omega}s + \hat{\omega}^2}\ \{\tilde{\mathbf{X}}_t\} \text{ and } \tilde{Z}_r(s) = \frac{\hat{\omega}^2}{s^2 + 2\hat{\xi}\,\hat{\omega}s + \hat{\omega}^2}\ \{\tilde{\mathbf{X}}_r\} \tag{48}$$

where $\tilde{Z}(s)$ and $\tilde{Z}_r(s)$ are the Laplace transforms of Z and Z_r, respectively. Using Eqs. (45) and (46) in Eqs. (41) and (42), the open loop governing equations of motion in Laplace domain are augmented as follows:

$$s^2[\mathbf{M}]\{\tilde{\mathbf{X}}_t\} + \mathcal{L}([\mathbf{K}_{tt}]\{\mathbf{X}_t\} + [\mathbf{K}_{tr}]\{\mathbf{X}_r\}) + [\mathbf{K}_{tsv}]G^{\infty}(1+\alpha)\{\tilde{\mathbf{X}}_t\} - [\mathbf{K}_{tsv}]\ G^{\infty}\alpha\{\tilde{Z}(s)\} + [\mathbf{K}_{trsv}]G^{\infty}(1+\alpha)\{\mathbf{X}_r\} - [\mathbf{K}_{trsv}]\ G^{\infty}\alpha\{\tilde{Z}_r(s)\} = \{\tilde{\mathbf{F}}\} + \{\mathbf{F}_{tp}\}\tilde{V} + \mathcal{L}(\{\mathbf{F}_{tpn}\}) \quad (49)$$

$$\mathcal{L}([\mathbf{K}_{rt}]\{\mathbf{X}_t\}) + [\mathbf{K}_{rr}]\{\tilde{\mathbf{X}}_r\} + [\mathbf{K}_{trsv}]^T G^{\infty}(1+\alpha)\{\tilde{\mathbf{X}}_t\} - [\mathbf{K}_{trsv}]^T G^{\infty}\alpha\{\tilde{Z}(s)\} + +[\mathbf{K}_{rrsv}]^T G^{\infty}(1+\alpha)\{\tilde{\mathbf{X}}_t\} - [\mathbf{K}_{rrsv}]^T G^{\infty}\alpha\{\tilde{Z}(s)\} = \{\tilde{\mathbf{F}}\} + \{\mathbf{F}_{tp}\}\tilde{V} \quad (50)$$

Taking inverse Laplace transforms of Eqs. (48) - (50) and condensing the global degrees of freedom $\{\mathbf{X}_r\}$ from the resulting equations in the time domain, the following equations are obtained:

$$[\mathbf{M}]\{\ddot{\mathbf{X}}_t\} + [\mathbf{K}_x]\{\mathbf{X}_t\} + [\mathbf{K}_z]\{\mathbf{Z}\} + [\mathbf{K}_{zr}]\{\mathbf{Z}_r\} = \{\mathbf{F}\} + \{\mathbf{F}_p\}V \quad (51)$$

$$\{\ddot{\mathbf{Z}}\} + 2\hat{\xi}\hat{\omega}\{\dot{\mathbf{Z}}\} + \hat{\omega}^2\{\mathbf{Z}\} - \hat{\omega}^2\{\dot{\mathbf{X}}_t\} = \mathbf{0} \quad (52)$$

$$\{\ddot{\mathbf{Z}}_r\} + 2\hat{\xi}\hat{\omega}\{\dot{\mathbf{Z}}_\mathbf{r}\} + \hat{\omega}^2[\mathbf{K}_1]\{\tilde{\mathbf{X}}_t\} - \hat{\omega}^2[\mathbf{K}_2]\{\mathbf{Z}\} + \hat{\omega}^2[\mathbf{K}_3]\{\mathbf{Z}_r\} = \{\mathbf{F}_{Tz}\} + \{\mathbf{F}_{pz}\}V \quad (53)$$

where

$$[\mathbf{K}_x] = [\bar{\mathbf{K}}_{tt}] - [\bar{\mathbf{K}}_{tr}][\bar{\mathbf{K}}_{rr}]^{-1}[\bar{\mathbf{K}}_{rt}]\ ,$$
$$[\mathbf{K}_z] = [\bar{\mathbf{K}}_{tr}][\bar{\mathbf{K}}_{rr}]^{-1}[\mathbf{K}_{trsv}]^T G^{\infty}\alpha - [\mathbf{K}_{tsv}]\ G^{\infty}\alpha\ ,$$
$$[\mathbf{K}_{zr}] = [\bar{\mathbf{K}}_{tr}][\bar{\mathbf{K}}_{rr}]^{-1}[\mathbf{K}_{rrsv}]\ G^{\infty}\alpha - [\mathbf{K}_{trsv}]\ G^{\infty}\alpha,$$
$$\{\mathbf{F}_p\} = \{\mathbf{F}_{tp}\} + \{\mathbf{F}_{tpn}\} + [\bar{\mathbf{K}}_{tr}][\bar{\mathbf{K}}_{rr}]^{-1}\{\mathbf{F}_{rp}\},$$
$$\{\mathbf{F}\} = \{\mathbf{F}_t\} + [\bar{\mathbf{K}}_{tr}][\bar{\mathbf{K}}_{rr}]^{-1}\{\mathbf{F}_T\} + \{\mathbf{F}_{Tb}\} + [\bar{\mathbf{K}}_{tr}][\bar{\mathbf{K}}_{rr}]^{-1}\{\mathbf{F}_{Tr}\},$$
$$[\mathbf{K}_1] = [\bar{\mathbf{K}}_{rr}]^{-1}[\bar{\mathbf{K}}_{rt}]\ ,\ [\mathbf{K}_2] = [\bar{\mathbf{K}}_{rr}]^{-1}[\mathbf{K}_{trsv}]^T G^{\infty}\alpha\ ,$$
$$[\mathbf{K}_3] = I_{zr} - [\bar{\mathbf{K}}_{rr}]^{-1}[\mathbf{K}_{rrsv}]\ G^{\infty}\alpha\ ,\{\mathbf{F}_{pz}\} = \hat{\omega}^2[\bar{\mathbf{K}}_{rr}]^{-1}\{\mathbf{F}_{rp}\}$$
$$[\bar{\mathbf{K}}_{tt}] = [\mathbf{K}_{tt}] + [\mathbf{K}_{tsv}]G^{\infty}(1+\alpha)\,,$$
$$[\bar{\mathbf{K}}_{tr}] = [\mathbf{K}_{tr}] + [\mathbf{K}_{trsv}]\ G^{\infty}(1+\alpha)$$
$$[\bar{\mathbf{K}}_{rt}] = [\mathbf{K}_{rt}] + [\mathbf{K}_{trsv}]^T G^{\infty}(1+\alpha),$$
$$[\bar{\mathbf{K}}_{rr}] = [\mathbf{K}_{rr}] + [\mathbf{K}_{rrsv}]G^{\infty}(1+\alpha) \quad (54)$$

Now, Eqs. (51) – (53) are combined to obtain the global open-loop equations of motion in the time domain as follows:

$$[\mathbf{M}^*]\{\ddot{\mathbf{X}}\} + [\mathbf{C}^*]\{\dot{\mathbf{X}}\} + [\mathbf{K}^*]\{\mathbf{X}\} = \{\mathbf{F}^*\} + \{\mathbf{F}_p^*\}\mathbf{V} \quad (55)$$

in which

$$[\mathbf{M}^*] = \begin{bmatrix}[\mathbf{M}] & 0 & 0\\ 0 & I_z & 0\\ 0 & 0 & I_{zr}\end{bmatrix}, [\mathbf{C}^*] = \begin{bmatrix}0 & 0 & 0\\ 0 & 2\hat{\xi}\hat{\omega} & 0\\ 0 & 0 & 2\hat{\xi}\hat{\omega}\end{bmatrix},$$

$$[\mathbf{K}^*] = \begin{bmatrix}[\mathbf{K}_x] & [\mathbf{K}_z] & [\mathbf{K}_{zr}]\\ -\hat{\omega}^2 & \hat{\omega}^2 & 0\\ \hat{\omega}^2[\mathbf{K}_1] & -\hat{\omega}^2[\mathbf{K}_2] & \hat{\omega}^2[\mathbf{K}_3]\end{bmatrix},$$

$$\{\mathbf{F}^*\} = \begin{Bmatrix}\{\tilde{\mathbf{F}}_t\}\\ 0\\ \{\mathbf{F}_{Tz}\}\end{Bmatrix},\ \{\mathbf{F}_p^*\} = \begin{Bmatrix}\{\mathbf{F}_p\}\\ 0\\ \{\mathbf{F}_{pz}\}\end{Bmatrix}\ \text{and}\ \{\mathbf{X}\} = \begin{Bmatrix}\{\mathbf{X}_t\}\\ Z\\ Z_r\end{Bmatrix} \quad (56)$$

CLOSED LOOP MODEL

In order to apply the control voltage for activating the patches of the ACLD treatment, a simple velocity feedback control law has been employed. According to this law, the control voltage for each patch can be expressed in terms of the derivatives of the global nodal degrees of freedom as follows:

$$V^j = -K_d^j\,\dot{w} = -K_d^j[\mathrm{U}^j]\{\dot{\mathrm{X}}\} \quad (57)$$

in which K_d^j is the control gain for the j^{th} patch and $[\mathrm{U}^j]$ is a unit vector defining the location of sensing the velocity signal. Finally, substituting Eq.(57) into Eq.(55), the equations of motion governing the closed loop nonlinear dynamics of the FG sandwich plates activated by the patches of the ACLD treatment can be obtained as follows:

$$[\mathrm{M}^*]\{\ddot{\mathrm{X}}\} + [\mathrm{C}_d{}^*]\{\dot{\mathrm{X}}\} + [\mathrm{K}^*]\{\mathrm{X}\} = \{\mathrm{F}^*\} \quad (58)$$

where, $[\mathrm{C}_d{}^*] = [\mathrm{C}^*] + \sum_{j=1}^{m} K_d^j\{\mathrm{F}_p^*\}[\mathrm{U}^j]$ is an active damping matrix and m is the number of ACLD patches

RESULTS AND DISCUSSIONS

In this section, numerical results are computed by the finite element model derived in the previous section for assessing the performance of the ACLD patches on controlling the geometrically nonlinear vibrations of $1-1-1$ ($2h_c/h_f = 1$)and $1-2-1$ ($h_c/h_f = 1$)FG sandwich plates with Flexible HEREX core configurations. The $1-1-1$ FG sandwich plate signifies that all the layers of the plate are of equal thickness. Unless otherwise mentioned, the bottom facing and the top facing of the substrate sandwich plate are ceramic-metal FGM while the top surface of the top facing and the bottom surface of the bottom facings are metal rich. The top surface of the top facing of the FG sandwich plate are integrated with two patches of the ACLD treatment located at the edges of the plate as shown in Fig.1 (b). The material properties of the core and the constituents of the top and the bottom facings of the substrate sandwich plate within the temperature range of $300K - 800K$ are as follows [51].

HEREX Core(C70.130) [4]

$E = 0.10363\ GPa, \upsilon = 0.33; \rho = 130\ \mathrm{Kg/m^3}$

Aluminum:

$$E(T) = 74 + 23\times10^{-3}T - 11\times10^{-5}T^2 + 51\times10^{-9}T^3,$$
$$\alpha(T) = 1.6\times10^{-5} + 3.45\times10^{-8}T - 3.3\times10^{-11}T^2 + 2.4\times10^{-14}T^3, k = 218 \quad (59)$$

Zirconia:

$$E(T) = 225 - 20\times10^{-2}T + 90\times10^{-6}T^2 + 4\times10^{-9}T^3,$$
$$\alpha(T) = 1.48\times10^{-5} - 2.2\times10^{-8}T + 1.15\times10^{-11}T^2 + 4\times10^{-14}T^3,$$
$$k(T) = 11\times10^{-1} + 16\times10^{-5}T + 19\times10^{-7}T^2 - 97\times10^{-11}T^3 \quad (60)$$

The poissons ratio for the aluminum and zirconia are considered to be 0.3. The variations of the normalized young's modulus (E_{fg}/E_c) of the FG substrate plate along the thickness direction

of the facings for different values of the power-law index are shown in Fig. 3 when the top and bottom surfaces of the plate are metal rich.

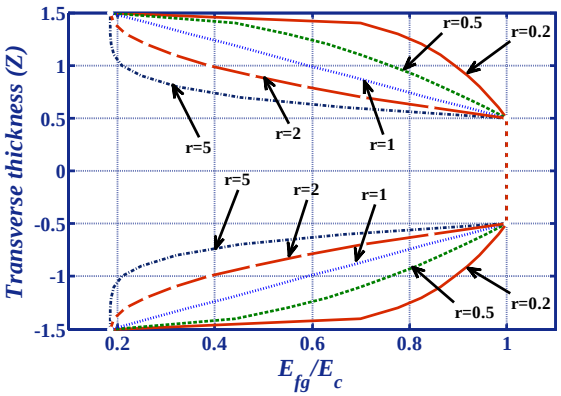

Figure 3. VARIATION OF NORMALIZED YOUNG'S MODULUS ACROSS THE THICKNESS OF THE FACINGS OF $1-1-1$ FG SANDWICH PLATE FOR DIFFERENT POWER-LAW INDICES OF METAL RICH TOP AND BOTTOM SURFACES

The length and the width of the patches are 50% and 25% of the length and the width of the sandwich plate, respectively. PZT-5 H/spur epoxy composite with 60% piezoelectric fiber volume fraction has been considered for the material of the constraining layer of the ACLD treatment. The elastic and the piezoelectric properties of this constraining layer are [27]:

$C^p_{11} = 9.29$ GPa, $C^p_{12} = 6.18$ GPa, $C^p_{13} = 6.05$ GPa, $C^p_{33} = 35.44$ GPa, $C^p_{23} = C^p_{13}$, $C^p_{44} = 1.58$ GPa, $C^p_{55} = 1.54$ GPa, $C^p_{55} = C^p_{44}$, $e_{31} = -0.1902$ C/m^2, $e_{33} = 18.4107$ C/m^2

The thicknesses of the constraining 1–3 PZC layer and the viscoelastic layer are considered to be 250 μm, 200 μm, respectively. Unless otherwise mentioned, the aspect ratio (a/H) and the thickness of the substrate sandwich plate are considered as 150 and 0.003 m, respectively. Also unless otherwise mentioned, the piezoelectric fiber orientation angle (Ψ) in the PZC patches is considered to be 0° and the mechanical pulse load (P) acting upward is assumed to be uniformly distributed. Considering a single term GHM expression, the values of α, $\hat{\omega}$ and $\hat{\xi}$ are used as 11.42, 1.0261x 10^5 and 20, respectively [43]. The shear modulus (G^{∞}) and the density of the viscoelastic material (ρ_V) are used as 1.822×10^6 Pa and 1104 kg/m^3, respectively [43]. The simply supported type-1 (SS1) boundary conditions at the edges of the overall sandwich plate considered for evaluating the numerical results are given by

$v_0 = w_0 = \theta_y = \phi_y = \alpha_y = \beta_y = \gamma_y = \theta_z = \phi_z = \alpha_z = \beta_z = \gamma_z = 0$, at $x=0, a$ and

$u_0 = w_0 = \theta_x = \phi_x = \alpha_x = \beta_x = \gamma_x = \theta_x = \phi_z = \alpha_z = \beta_z = \gamma_z = 0$, at $y=0, b$ (61)

Following the approach by Lim et al. [50], first the validity of the implementation of the GHM method for modeling the ACLD treatment is checked. For this, simply supported FG sandwich plates integrated with the ACLD patches as shown in Fig. 1(b) are considered. The linear frequency responses for the transverse displacement of these substrate sandwich plates are evaluated when the viscoelastic material is modeled by the GHM method and the conventional complex modulus approach, separately. A transverse pulse pressure loading of 4000 N/m^2 is considered to excite the first few modes of both the substrate sandwich plates. Figure 4 illustrate these frequency response functions for the sandwich plates with flexible HEREX (C70 130) core. It may be clearly observed from Fig. 4 that the frequency response curves obtained by the two approaches are almost overlapping with one another. Thus, it may be concluded that the present method of modeling the viscoelastic material by the GHM method accurately predicts the damping characteristics of the overall smart FG sandwich plates.

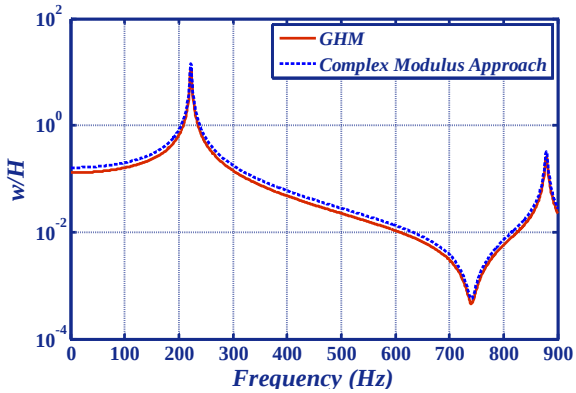

Figure 4. LINEAR FREQUENCY RESPONSES FOR CENTRAL DEFLECTION OF A SIMPLY-SUPPORTED $1-1-1$ (FG/HEREX (C70 130)/FG) SANDWICH PLATE OBTAINED BY THE GHM METHOD AND THE COMPLEX MODULUS APPROACH $(a/H = 200, r = 2, T_c = 400, T_m = 300)$.

In order to further verify the accuracy of the current numerical model, the fundamental natural frequencies of the FG sandwich plates studied by Zenkour [20] are computed by the present FE model and compared with those obtained by Zenkour [20] as shown in Table 1. It is evident that the two sets of results are in good agreement with each other.

Table-1 Fundamental natural frequency of simply-supported (SS1) square FG sandwich plate evaluated by present finite element model with $a/b = 1, a/H = 10$.

Power-law index 'r'	Type of FG plate	Ref. [20]	Present FE soln.
0.5	$1-2-1$	1.57274	1.54321
	$1-1-1$	1.51695	1.53062
1	$1-2-1$	1.43722	1.43513
	$1-1-1$	1.35072	1.35816
5	$1-2-1$	1.17159	1.17154
	$1-1-1$	1.04183	1.03988

$\left(\bar{\omega} = \frac{\omega a^2}{H}\sqrt{\frac{\rho_0}{E_0}}\right), E_0 = 1$GPa and $\rho_0 = 1$ kg/m^3

The open- and closed-loop behavior of the substrate FG sandwich plates with the HEREX (C70 130) core configuration are studied by computing the transverse deflection at the centre $(a/2, b/2, H/2)$ of the top surface of the plates. A uniformly distributed transverse pulse load is applied to set the overall plate into motion. For a considerable amount of nonlinearity to be present in the response, the amplitude ratio has been maintained to be always greater than 1.5 $(w/H \geq 1.5)$. The control voltage supplied to each ACLD patch is negatively

proportional to the velocity of the point located on the plate outer surface which corresponds to the midpoint of the free length of the patch. The control gain is chosen arbitrarily such that the nonlinear vibrations of the plates are under control and the maximum control voltage supplied does not exceed a nominal value of 300 Volt. Figure 5 illustrate the nonlinear transient response of the FG/HEREX C70 130/FG symmetric substrate sandwich plates subjected to different temperature fields at the bottom surface of the bottom layer and at the interface of the bottom layer and the core, respectively. The control voltages corresponding to the gain used are quite nominal as shown in Fig. 6 for controlling the geometrical non-linear vibrations of the sandwich plates.

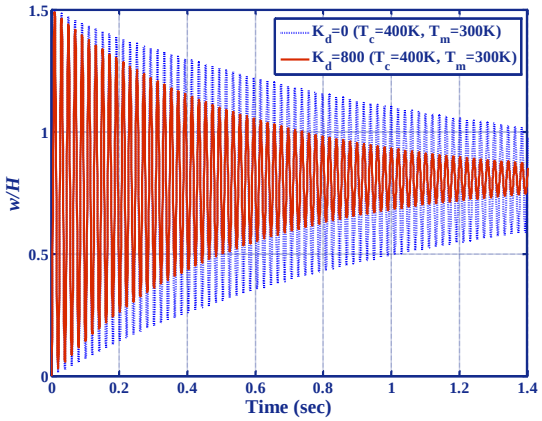

Figure 5. NONLINEAR TRANSIENT RESPONSES OF A SIMPLY-SUPPORTED $1-1-1$ FG/HEREX C70 130/FG SANDWICH PLATE UNDERGOING ACLD .

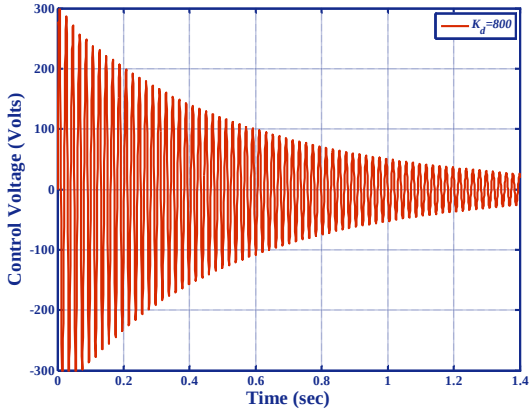

Figure 6. CONTROL VOLTAGES REQUIRED FOR THE ACLD OF NONLINEAR TRANSIENT VIBRATIONS OF THE SIMPLY-SUPPORTED $1-1-1$ FG/HEREX C70 130/FG SANDWICH PLATE.

The responses displayed in the Fig. 5 correspond to the cases when the ACLD patch is passive ($K_d = 0$) and active($K_d \neq 0$). It is evident from these figures that the active ACLD patches has a significant effect on the control of nonlinear transient vibrations of the FG sandwich plates and improves the damping characteristics of the overall plate over the passive damping. Since the control voltage is proportional to the velocity of the point on the plate, the illustrations of the control voltages in Fig. 6 indicate that at any point of the overall plate, the velocity also decays with time. The phase plot presented in Fig. 7 corroborates the same indicating the stability of the sandwich plate.

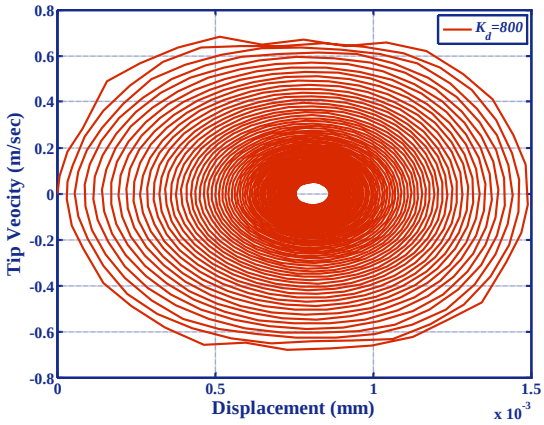

Figure 7. PHASE PLOT OF THE SIMPLY-SUPPORTED $1-1-1$ FG/HEREX C70 130/FG SANDWICH PLATE WHEN THE ACLD PATCHES CONTROL THE NONLINEAR VIBRATIONS.

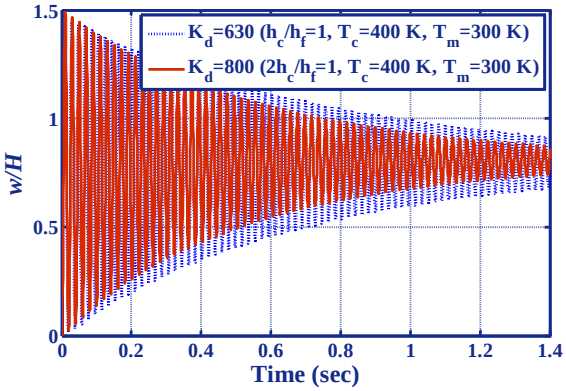

FIGURE 8. NONLINEAR TRANSIENT RESPONSES OF A SIMPLY-SUPPORTED $1-1-1$ AND $1-2-1$ FG/HEREC C70 130/FG SANDWICH PLATES UNDERGOING ACLD

The controlled responses of simply-supported (**SS1**) **FG**/HEREX C70 130/**FG** sandwich plates with $1-1-1$ and $1-2-1$configurations for the same maximum amplitude ratio ($w/H = 1.5$) and same maximum control voltages (V=300 **Volt**) are illustrated in Fig. 8. It may be observed from these figures that for the same value of the maximum control voltage supplied, the time for damping the nonlinear vibrations of the 1-2-1 **FG**/HEREX C70 130/**FG** sandwich plate is more than that of the $1-1-1$ **FG**/HEREX C70 130/**FG** sandwich plate. Next, the controlled responses of simply-supported (SS1) FG/HEREX C70 130/FG sandwich plates for the same maximum amplitude ratio ($w/H = 1.5$) and same maximum control voltages (V=300 Volt) with metal rich bottom surface and ceramic rich bottom surface of the bottom layer exposed to temperature fields are illustrated in Fig. 9. It may be observed from the figure that for the same value of the maximum control voltage supplied, the time for damping the nonlinear vibrations of the FG sandwich plate with metal rich bottom surface is less as compared to that of the case with ceramic rich bottom surface. Figure 10 illustrates the transient responses of simply-supported FG sandwich plate when the bottom facing of the substrate is exposed to different temperature fields for the same applied transverse distributed pulse loading and same maximum

value of control voltages(V=300 Volt). It can be observed from the figure that as the difference in temperature $(T_c - T_m)$ increases, the value of amplitude ratio decreases and hence the damping time reduces. The corresponding control voltages for the responses in Fig. 10 are shown in Fig. 11.

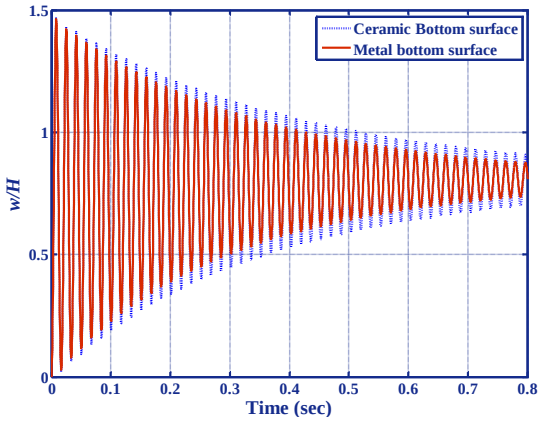

Figure 9. NONLINEAR TRANSIENT RESPONSES OF A SIMPLY-SUPPORTED $1-1-1$ FG/HEREX C70 130/FG SANDWICH PLATE UNDERGOING ACLD $(T_c = 500, T_m = 300)$

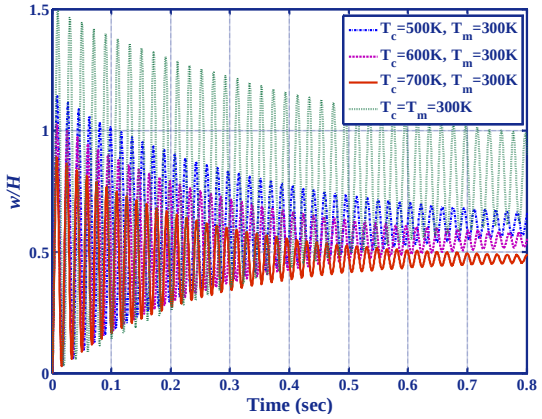

Figure 10. ACLD OF GEOMETRICALLY NONLINEAR VIBRATIONS OF A SIMPLY-SUPPORTED 1-1-1 FG/HEREX C70 130/FG PLATE WITH DIFFERENT COMBINATIONS OF TOP AND BOTTOM SURFACES $(P = 5000\ N/m^2,\ r = 1)$.

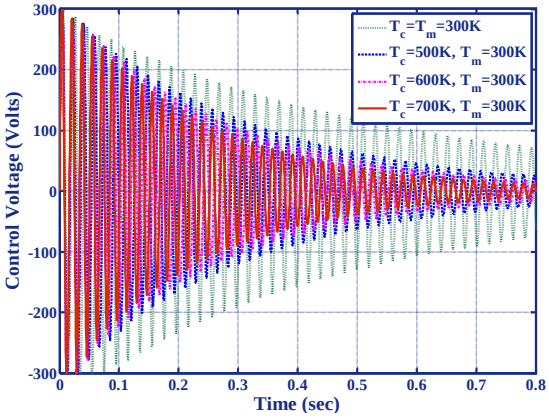

Figure 11. CONTROL VOLTAGES REQUIRED FOR THE ACLD OF NONLINEAR VIBRATIONS OF THE SIMPLY-SUPPORTED 1-1-1 FG/HEREX C70 130/FG WITH DIFFERENT COMBINATIONS OF TOP AND BOTTOM SURFACES $(P = 1000\ N/m^2, r = 2)$

In order to investigate the effect of the variation of the piezoelectric fiber orientation angle (Ψ) in the obliquely reinforced 1-3 **PZC** constraining layer of the **ACLD** patch on the control authority of the patch, the fiber orientation angle (Ψ) is varied from $-45^o\ to\ 45^o$ in both the $xz-$ and the $yz-$planes. A performance index (I_d) for evaluating the control authority of the obliquely reinforced 1-3 **PZC** constraining layer is defined as follows:

$$I_d = \frac{w\left(\frac{a}{2},\frac{b}{2},\frac{H}{2},0\right) - w\left(\frac{a}{2},\frac{b}{2},\frac{H}{2},t\right)}{w\left(\frac{a}{2},\frac{b}{2},\frac{H}{2},0\right)} \times 100 \qquad (62)$$

Here, I_d measures the percentage diminution of the displacement at the point $(a/2, b/2, H/2)$ of the controlled FG sandwich plate undergoing nonlinear transient vibrations after 0.5 s. For a particular value of the maximum control voltage (V=300 Volt), Fig. 12 illustrate the variation of the performance index I_d of the ACLD patch with the piezoelectric fiber orientation angle (Ψ) of simply supported (SS1) $1-1-1$FG/HEREX C70 130/FG sandwich plate. It may be observed that for the FG sandwich plate, the performance index I_d becomes maximum when the value of the piezoelectric fiber orientation angle (Ψ) is 0^o in the $xz-$plane irrespective of the value of the power-law index. Similar results are found when the piezoelectric fiber orientation angle is varied in the $yz-$plane. However, for the sake of brevity they are not presented here.

The damping ratio of $1-1-1$ FG/HEREX C70 130/FG sandwich plates studied here are also determined. For a considerable amount of accuracy, the damped response amplitudes are computed for 20 cycles and the corresponding logarithmic decrement is found which has been used to compute the damping ratio $\boldsymbol{\zeta}$ and the value obtained is of the order $\boldsymbol{\zeta} = 0.003457$. Also, the damping ratio concerning the GHM method and complex modulus approach for the fundamental mode is of the order $\boldsymbol{\zeta_{GHM}} = 0.002436$ and $\boldsymbol{\zeta_{complex}} = 0.002215$.

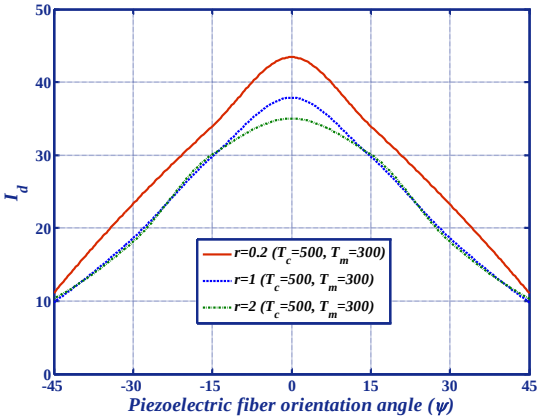

Figure 12. EFFECT OF VARIATION OF PIEZOELECTRIC FIBER ORIENTATION ANGLE (Ψ) IN THE 1-3 PZC CONSTRAINING LAYER OF THE ACLD PATCH WHEN THE FIBERS ARE COPLANAR WITH THE $xz-$PLANE FOR THE SIMPLY-SUPPORTED $1-1-1$ (FG/HEREX C 70 130/FG) SANDWICH PLATE $(max(V) = 300\ Volts, a/H = 200)$.

5. CONCLUSIONS

In this paper, a three dimensional finite element analysis has been carried out to investigate the performance of the patches of

the ACLD treatment for controlling geometrically nonlinear vibrations of FG sandwich plates with the bottom layer exposed to temperature field. The constraining layer of the ACLD patch is considered to be made of the vertically/obliquely reinforced 1-3 PZC. The kinematics of deformations of the individual layers of the overall FG sandwich plate is assumed to be based on the first order shear deformation theory and the von Kármán type strain-displacement relations are used for modeling the geometric nonlinearity. The viscoelastic layer is modeled by using the GHM approach, which is a time domain formulation. A simple velocity feedback control law is used to introduce the active damping. FG sandwich plates with flexible honeycomb core with the bottom surface of the bottom facing exposed to different temperatures while the interface between the bottom facing and the core is at room temperature are considered for evaluating the numerical results. The geometrically nonlinear dynamics of the FG sandwich plates subjected to temperature field are of hardening type. The numerical results for controlled responses reveal that the ACLD treatment significantly improves the active damping characteristics of the FG sandwich plates over the passive damping for suppressing their geometrically nonlinear transient vibrations. The controllability of the ACLD patches increases with the increase in the value of power-law index. For active damping of geometrically nonlinear vibrations of the FG sandwich plates the contribution of vertical actuation by the vertically reinforced 1-3 PZC layer is significantly larger than that of the in-plane actuation by the same. The performance of ACLD patches becomes maximum when the patches are vertically aligned ($\Psi = 0^o$) in the constraining layer for sandwich plates with flexible honeycomb core irrespective of the value of the power-law index.

REFERENCES

1. Zenkert, D., 1995 "An Introduction to Sandwich Construction." London: Chameleon Press.
2. Noor, A. K., Burton, W. S. and Bert, C. W., 1996. "Computational models for sandwich panels and shells". *Applied Mechanics Reviews, Transactions of ASME*, **49(3)**, April, pp. 155–199.
3. Sokolinsky, V. and Frostig, Y., 2000. "Branching behavior in the non-linear response of sandwich panels with a transversely flexible core". *International Journal of Solids and Structures*, **37**, October, pp. 5745–5772.
4. Nayak, A. K., Moy, S. S. J. and Shenoi, R. A., 2002. "Free vibration analysis of composite sandwich plates based on Reddy's higher-order theory". *Composites: Part B*, **33**, October, pp. 505-519.
5. Oded, R., Jack, R. V. and Yeoshua F., 2003 "High-Order Analysis of Unidirectional Sandwich Panels with Piezolaminated Face Sheets and Soft Core". *AIAA Journal*, **41(1)**, January, pp. 110-118.
6. Altenbach, H., Altenbach, J. and Kissing, W., 2004. "Mechanics of Composite Structural Elements". *Springer-Verlag*, Berlin.
7. Khare, R. K., Garg, A. K. and Kant. T., 2005. "Free vibration of sandwich laminates with two higher-order shear deformable facet shell element models", *Journal of Sandwich Structures and Materials*, **7(6)**, May, pp. 221-244
8. Frostig, Y. and Thomsen, O. T., 2008. "Non-linear thermal response of sandwich panels with a flexible core and temperature dependent mechanical properties". *Composites Part B*: *Engineering*, **39(1)**, January, pp. 165-184.
9. Burlayenko, V. and Sadowski, T., 2009. "Analysis of structural performance of aluminum sandwich plates with foam-filled hexagonal honeycomb core", *Computational Material Science*, **45**, May, pp. 658–662.
10. Yamanouchi, M., Koizumi, M., Hirai, T. and Shiota, I., 1990. "Proceedings of the first international symposium on functionally gradient materials", October, Sendai, Japan.
11. Koizumi, M., 1993. "Concept of FGM", *Ceramic Transactions*, **34**, pp. 3-10.
12. Feldman, E. and Aboudi, J., 1997. "Buckling analysis of functionally graded plates subjected to uniaxial loading", *Composite Structures*, **38**, May, pp. 29–36.
13. Loy, C. T., Lam, K. Y. and Reddy, J. N., 1999. "Vibration of functionally graded cylindrical shells", *International Journal of Mechanical Sciences*, **41**, March, pp. 309–324.
14. Zenkour, A. M., 1999. "Transverse shear and normal deformation theory for bending analysis of laminated and sandwich elastic beams", *Mechanics of Composite Materials and Structures*, **6**, pp. 267-283.
15. Reddy, J. N., 2000. "Analysis of functionally graded plates", *International Journal of Numerical Methods in Engineering*, **47**, June, pp. 663-684.
16. Sankar, B.V., 2001. "An elasticity solution for functionally graded beams", *Composite Science and Technology*, **61 (5)**, April, pp. 689–696.
17. Vel, S. S. and Batra, R. C., 2003. "Three-dimensional analysis of transient thermal stresses in functionally graded plates", *International Journal of Solids and Structures*, **40**, pp. 7181–7196.
18. Zenkour, A. M., 2005. "A comprehensive analysis of functionally graded sandwich plates: Part 1- Deflection and stresses", *International Journal of Solids and Structures*, **42**, September, pp. 5224-5242.
19. Zenkour, A. M., 2005 "A comprehensive analysis of functionally graded sandwich plates: Part -2 Buckling and free vibration", *International Journal of Solids and Structures*, **42**, September, pp. 5242-5258.
20. Zenkour, A. M., 2006. "Generalized shear deformation theory for bending analysis of functionally graded plates", *Applied Mathematical Modelling*, 30, January, pp. 67-84.
21. Bailey, T. and Hubbard, J.E., 1985. "Distributed piezoelectric polymer active vibration control of a cantilever beam", *Journal of Guidance, Control and dynamics*, **8**, October, pp. 605–611.

22. Baz, A. and Poh, S., 1988. “Performance of an active control system with piezoelectric actuators”, *Journal Sound and Vibration*, **126**, October, pp. 327–343.

23. Smith, W.A. and Auld, B.A., 1991. “Modelling 1-3 composite piezoelectrics: thickness mode oscillations”, *IEEE Transactions. Ultrasonics and Ferroelectrics. Frequency and control*, **31**, January, pp. 40-47.

24. Ghosh, K. and Batra, R.C., 1995. “Shape control of plates using piezoceramic elements”, *AIAA Journal*, 33(7), February, pp. 1354–1357.

25. Ray, M.C. and Sachade, H.M., 2005. “Exact solutions for the functionally graded plates integrated with a layer of piezoelectric fiber-reinforced composite”, *ASME Journal of Applied Mechanics*, 73(4), April, pp. 622-632.

26. Baz, A., 1996. “Active constrained layer damping”, U.S. patent 5, 485,053.

27. Dunn, M. L. and Taya, M., 1993. “Micromechanics predictions of the effective electro elastic modulli of piezoelectric composites”, *International Journal of Solids and Structures*, **30**, pp. 161–175.

28. Aboudi, J., 1998. “Micromechanical prediction of the effective coefficients of thermo-piezoelectric multiphase composites”, *Journal of Intelligent Material Systems and Structures*, 9, September, pp. 713–722.

29. Arafa, M. and Baz, A., 2000. “Dynamics of active piezoelectric damping composites”, *Composites: Part B*, **31**, June, pp. 255–264.

30. Piezocomposites, Materials Systems Inc., 543 Great Road, Littleton, MA 01460.

31. Ray, M.C. and Pradhan, A.K., 2006. “Performance of vertically reinforced 1–3 piezoelectric composites for active damping of smart structures”, *Smart Materials and Structures*, **15 (1)**, April, pp. 631–641.

32. Ray, M.C., and Pradhan, A.K., 2007. “On the use of vertically reinforced 1–3 piezoelectric composites for hybrid damping of laminated composite plates”, *Mechanics of Advanced Materials and Structures*, **14 (4)**, May, pp. 245–261.

33. Reddy, J. N., 1983 “Geometrically nonlinear transient analysis of laminated composite plates”, *AIAA Journal*, **21(4)**, April, pp. 621–629.

34. Ganapathi, M., Varadan, T. K. and Sarma, B. S., 1991. “Nonlinear flexural vibrations of laminated orthotropic plates”, *Computers and Structures*, **39**, pp. 685-688.

35. Kant, T. and Kommineni, J. R., 1994. “Large amplitude free vibration analysis of cross-ply composite and sandwich laminates with a refined theory and C^0 finite elements”, *Computers and Structures*, **50(1)**, pp. 123-134.

36. Praveen, G. N. and Reddy, J. N., 1998. “Nonlinear transient thermo elastic analysis of functionally graded ceramic metal plates”, *International Journal of Solids and Structures*, **35**, November, pp. 4457–4476.

37. Woo, J. and Meguid, S. A., 2001. “Nonlinear analysis of functionally graded plates and shallow shells”, *International Journal of Solids and Structures*, **38**, October, pp. 7409–7421.

38. Shen, H. S., 2002. “Nonlinear bending response of functionally graded plates subjected to transverse loads and in thermal environments”, *International Journal of Mechanical Sciences*, **44**, March, pp. 561–584.

39. Yang, J., Kitipornchi, S. and Liew, K. M., 2003. “Large amplitude vibration of thermo-electro-mechanically stressed FGM laminated plates”, *Computer Methods in Applied Mechanics and Engineering*, **192 (35)**, August, pp. 3861–3885.

40. Reddy, J. N., 2004. An Introduction to Nonlinear Finite Element Analysis, Oxford University Press Inc., New York.

41. Pai, P. F., Nayfeh, A. H., Oh, K. and Mook, D. T., 1993. “A Refined Nonlinear Model of Composite Plates with Integrated Piezoelectric Actuators and Sensors”, *International Journal of Solids and Structures*, **30**, pp. 1603-1630.

42. Ray, M. C. and Baz, A., 2001. “Control of Nonlinear Vibration of Beams Using Active Constrained Layer Damping Treatment”, *Journal of Vibration and Control*, **7**, May, pp. 539-549.

43. Reddy, J. N. and Cheng, Z. Q., 2001. “Three-dimensional solutions of smart functionally graded plates”, *ASME Journal of Applied Mechanics*, **68 (3)**, May, pp. 234–241.

44. Kulkarni, S. A. and Bajoria, K. M., 2006. “Geometrically Nonlinear Analysis of Smart Thin and Sandwich Plates”, *Journal of Sandwich Structures and Materials*, **8**, July, pp. 321-341.

45. Panda, S. and Ray, M. C., 2006. “Nonlinear analysis of smart functionally graded plates integrated with a layer of piezoelectric fiber reinforced composite”, *Smart Materials and Structures*, **15**, October, pp. 1595–1604.

46. Panda, S. and Ray, M. C., 2008. “Active constrained layer damping of geometrically nonlinear transient vibrations of smart functionally graded plates using piezoelectric fiber reinforced composite”, *Smart Materials and Structures*, **17,** Artno.025012.

47. Suresh Kumar, R. and Ray, M. C., 2012. “Active constrained layered damping of geometrically nonlinear vibrations of smart laminated composite sandwich plates using 1-3 piezoelectric composites, *International Journal of Mechanics and Materials in Design*, **8(4)**, September, pp. 359-380.

48. Golla, D. F. and Hughes, P. C., 1985. “Dynamics of viscoelastic structures: a time- domain, finite element formulation”, *ASME Journal of Applied Mechanics*, **52**, December, pp. 897–906.

49. McTavish, D. J. and Hughes, P. C., 1993. “Modeling of linear viscoelastic space structures”, *ASME Journal of Vibration and Acoustics*, **115**, January, pp. 103–133.

50. Lim, Y. H., Varadan Vasundara, V. V. and Vijay, K., 2002. "Closed loop finite element modeling of active constrained layer damping in the time domain analysis", *Smart Materials and Structures*, **11**, February, pp. 89–97.

51. Noda, N., 1999. "Thermal Stresses in Functionally Graded Materials", *Journal of Thermal Stresses*, 22, pp. 477-512.

Appendix:

In Eqs. (8) and (9) , the various matrices $[\mathbf{Z}_1]$, $[\mathbf{Z}_2]$, $[\mathbf{Z}_3]$, $[\mathbf{Z}_4]$, $[\mathbf{Z}_5]$, $[\mathbf{Z}_6]$, $[\mathbf{Z}_7]$, $[\mathbf{Z}_8]$, and $[\mathbf{Z}_9]$ are given by

$$[\mathbf{Z}_1] = \left[[\bar{\mathbf{Z}}_1] \;\; \tilde{\mathbf{0}} \;\; \tilde{\mathbf{0}} \;\; \tilde{\mathbf{0}} \;\; \tilde{\mathbf{0}}\right]$$

$$[\mathbf{Z}_2] = [(-\mathrm{h_c})\mathbf{I} \;\; [\bar{\mathbf{Z}}_2] \;\; \tilde{\mathbf{0}} \;\; \tilde{\mathbf{0}} \;\; \tilde{\mathbf{0}}]$$

$$[\mathbf{Z}_3] = [\,(h_c)\mathbf{I} \;\; \tilde{\mathbf{0}} \;\; [\bar{\mathbf{Z}}_3] \;\; \tilde{\mathbf{0}} \;\; \tilde{\mathbf{0}}]$$

$$[\mathbf{Z}_4] = [(\,h_c)\mathbf{I} \;\; \tilde{\mathbf{0}} \;\; (h)\mathbf{I} \;\; (h_v)\mathbf{I} \;\; [\bar{\mathbf{Z}}_5]]$$

$$[\mathbf{Z}_5] = [\bar{\mathbf{I}} \;\; \bar{\mathbf{0}} \;\; \bar{\mathbf{0}} \;\; \bar{\mathbf{0}} \;\; \bar{\mathbf{0}} \;\; z\bar{\mathbf{I}} \;\; \bar{\mathbf{0}} \;\; \bar{\mathbf{0}} \;\; \bar{\mathbf{0}} \;\; \bar{\mathbf{0}}]$$

$$[\mathbf{Z}_6] = [\bar{\mathbf{0}} \;\; \bar{\mathbf{I}} \;\; \bar{\mathbf{0}} \;\; \bar{\mathbf{0}} \;\; \bar{\mathbf{0}} \;\; (-h_c)\bar{\mathbf{I}} \;\; (z+h_c)\bar{\mathbf{I}} \;\; \bar{\mathbf{0}} \;\; \bar{\mathbf{0}} \;\; \bar{\mathbf{0}}]$$

$$[\mathbf{Z}_7] = [\bar{\mathbf{0}} \;\; \bar{\mathbf{0}} \;\; \bar{\mathbf{I}} \;\; \bar{\mathbf{0}} \;\; \bar{\mathbf{0}} \;\; (h_c)\bar{\mathbf{I}} \;\; \bar{\mathbf{0}} \;\; (z-h_c)\bar{\mathbf{I}} \;\; \bar{\mathbf{0}} \;\; \bar{\mathbf{0}}]$$

$$[\mathbf{Z}_8] = [\bar{\mathbf{0}} \;\; \bar{\mathbf{0}} \;\; \bar{\mathbf{0}} \;\; \bar{\mathbf{I}} \;\; \bar{\mathbf{0}} \;\; (h_c)\bar{\mathbf{I}} \;\; \bar{\mathbf{0}} \;\; (h)\bar{\mathbf{I}} \;\; (z-h_c-h)\bar{\mathbf{I}} \;\; \bar{\mathbf{0}}]$$

$$[\mathbf{Z}_9] = [\bar{\mathbf{0}} \;\; \bar{\mathbf{0}} \;\; \bar{\mathbf{0}} \;\; \bar{\mathbf{0}} \;\; \bar{\mathbf{I}} \;\; (h_c)\bar{\mathbf{I}} \;\; \bar{\mathbf{0}} \;\; (h)\bar{\mathbf{I}} \;\; h_v\bar{\mathbf{I}} \;\; (z-h_c-h-h_v)\bar{\mathbf{I}}]$$

Where

$$[\bar{\mathbf{Z}}_1] = \begin{bmatrix} z & 0 & 0 & 0 \\ 0 & z & 0 & 0 \\ 0 & 0 & z & 0 \\ 0 & 0 & 0 & 1 \end{bmatrix},$$

$$[\bar{\mathbf{Z}}_2] = \begin{bmatrix} (z-h_c) & 0 & 0 & 0 \\ 0 & (z-h_c) & 0 & 0 \\ 0 & 0 & (z-h_c) & 0 \\ 0 & 0 & 0 & 1 \end{bmatrix}$$

$$[\bar{\mathbf{Z}}_3] = \begin{bmatrix} (z+h_c) & 0 & 0 & 0 \\ 0 & (z+h_c) & 0 & 0 \\ 0 & 0 & (z+h_c) & 0 \\ 0 & 0 & 0 & 1 \end{bmatrix}$$

$$[\bar{\mathbf{Z}}_5] = \begin{bmatrix} (z-h_c-h-h_v) & 0 & 0 & 0 \\ 0 & (z-h_c-h-h_v) & 0 & 0 \\ 0 & 0 & (z-h_c-h-h_v) & 0 \\ 0 & 0 & 0 & 1 \end{bmatrix}$$

$$\mathbf{I} = \begin{bmatrix} 1 & 0 & 0 & 0 \\ 0 & 1 & 0 & 0 \\ 0 & 0 & 1 & 0 \\ 0 & 0 & 0 & 0 \end{bmatrix}, \quad \bar{\mathbf{I}} = \begin{bmatrix} 1 & 0 \\ 0 & 1 \end{bmatrix}, \quad \bar{\mathbf{0}} = \begin{bmatrix} 0 & 0 \\ 0 & 0 \end{bmatrix}, \quad \tilde{\mathbf{0}} = \begin{bmatrix} 0 & 0 & 0 & 0 \\ 0 & 0 & 0 & 0 \\ 0 & 0 & 0 & 0 \\ 0 & 0 & 0 & 0 \end{bmatrix}$$

The various submatrices $[\mathrm{B_{tbi}}]$, $[\mathrm{B_{rbi}}]$, $[\mathrm{B_{tsi}}]$, $[\mathrm{B_{2i}}]$ and $[\mathrm{B_{rsi}}]$ appearing in Eq. (30)

$$[\mathbf{B}_{tbi}] = \begin{bmatrix} \frac{\partial \mathrm{n_i}}{\partial \mathrm{x}} & 0 & 0 \\ 0 & \frac{\partial \mathrm{n_i}}{\partial \mathrm{y}} & 0 \\ \frac{\partial \mathrm{n_i}}{\partial \mathrm{y}} & \frac{\partial \mathrm{n_i}}{\partial \mathrm{x}} & 0 \\ 0 & 0 & 0 \end{bmatrix}, \quad [\mathbf{B}_{tsi}] = \begin{bmatrix} 0 & 0 & \frac{\partial \mathrm{n_i}}{\partial \mathrm{x}} \\ 0 & 0 & \frac{\partial \mathrm{n_i}}{\partial \mathrm{y}} \end{bmatrix}, \quad [\mathbf{B}_{2i}] = \begin{bmatrix} 0 & 0 & \frac{\partial \mathrm{n_i}}{\partial \mathrm{x}} \\ 0 & 0 & \frac{\partial \mathrm{n_i}}{\partial \mathrm{y}} \end{bmatrix},$$

$$[\mathbf{B}_{\mathrm{rbi}}] = \begin{bmatrix} \widehat{\mathbf{B}_{rbi}} & \breve{\mathbf{0}} & \breve{\mathbf{0}} & \breve{\mathbf{0}} & \breve{\mathbf{0}} \\ \breve{\mathbf{0}} & \widehat{\mathbf{B}_{rbi}} & \breve{\mathbf{0}} & \breve{\mathbf{0}} & \breve{\mathbf{0}} \\ \breve{\mathbf{0}} & \breve{\mathbf{0}} & \widehat{\mathbf{B}_{rbi}} & \breve{\mathbf{0}} & \breve{\mathbf{0}} \\ \breve{\mathbf{0}} & \breve{\mathbf{0}} & \breve{\mathbf{0}} & \widehat{\mathbf{B}_{rbi}} & \breve{\mathbf{0}} \\ \breve{\mathbf{0}} & \breve{\mathbf{0}} & \breve{\mathbf{0}} & \breve{\mathbf{0}} & \widehat{\mathbf{B}_{rbi}} \end{bmatrix}, \quad \widehat{\mathbf{B}_{\mathrm{rbi}}} = \begin{bmatrix} \frac{\partial \mathrm{n_i}}{\partial \mathrm{x}} & 0 & 0 \\ 0 & \frac{\partial \mathrm{n_i}}{\partial \mathrm{y}} & 0 \\ \frac{\partial \mathrm{n_i}}{\partial \mathrm{y}} & \frac{\partial \mathrm{n_i}}{\partial \mathrm{x}} & 0 \\ 0 & 0 & 1 \end{bmatrix},$$

$$\breve{\mathbf{0}} = \begin{bmatrix} 0 & 0 & 0 \\ 0 & 0 & 0 \\ 0 & 0 & 0 \\ 0 & 0 & 0 \end{bmatrix},$$

$$[\mathbf{B}_{rsi}] = \begin{bmatrix} \check{\mathbf{I}} & \ddot{\mathbf{0}} & \ddot{\mathbf{0}} & \ddot{\mathbf{0}} & \ddot{\mathbf{0}} \\ \ddot{\mathbf{0}} & \check{\mathbf{I}} & \ddot{\mathbf{0}} & \ddot{\mathbf{0}} & \ddot{\mathbf{0}} \\ \ddot{\mathbf{0}} & \ddot{\mathbf{0}} & \check{\mathbf{I}} & \ddot{\mathbf{0}} & \ddot{\mathbf{0}} \\ \ddot{\mathbf{0}} & \ddot{\mathbf{0}} & \ddot{\mathbf{0}} & \check{\mathbf{I}} & \ddot{\mathbf{0}} \\ \ddot{\mathbf{0}} & \ddot{\mathbf{0}} & \ddot{\mathbf{0}} & \ddot{\mathbf{0}} & \check{\mathbf{I}} \end{bmatrix}, \quad \widehat{\mathbf{B}_{rsi}} = \begin{bmatrix} 0 & 0 & \frac{\partial \mathrm{n_i}}{\partial \mathrm{x}} \\ 0 & 0 & \frac{\partial \mathrm{n_i}}{\partial \mathrm{y}} \end{bmatrix},$$

$$\ddot{\mathbf{0}} = \begin{bmatrix} 0 & 0 & 0 \\ 0 & 0 & 0 \end{bmatrix}$$

The various rigidity matrices and the rigidity vectors for electro-elastic coupling elemental matrices appearing in Eqs. (33) and (34) are given by

$$\left[\mathbf{D}_{tb}^{b}\right] = \int_{h_0}^{h_1}[\mathbf{C}_b]_m \left[1+\left(\frac{E_c}{E_m}-1\right)V^{(1)}\right]\mathrm{dz},$$

$$\left[\mathbf{D}_{trb}^{b}\right] = \int_{h_0}^{h_1}[\mathbf{C}_b]_m \left[1+\left(\frac{E_c}{E_m}-1\right)V^{(1)}\right][Z_1]\mathrm{dz},$$

$$[\mathbf{D}_{ts}^{b}] = \int_{h_0}^{h_1}[\mathbf{C}_s]_m \left[1+\left(\frac{E_c}{E_m}-1\right)V^{(1)}\right]\mathrm{dz},$$

$$[\mathbf{D}_{trs}^{b}] = \int_{h_0}^{h_1}[\mathbf{C}_s]_m \left[1+\left(\frac{E_c}{E_m}-1\right)V^{(1)}\right][Z_5]\,\mathrm{dz},$$

$$\left[\mathbf{D}_{rrb}^{b}\right] = \int_{h_0}^{h_1}[\mathbf{Z}_1]^T[\mathbf{C}_s]_m \left[1+\left(\frac{E_c}{E_m}-1\right)V^{(1)}\right][\mathbf{Z}_1]\,\mathrm{dz},$$

$$[\mathbf{D}_{rrs}^{b}] = \int_{h_0}^{h_1}[\mathbf{Z}_5]^T[\mathbf{C}_s]_m \left[1+\left(\frac{E_c}{E_m}-1\right)V^{(1)}\right][\mathbf{Z}_5]\,\mathrm{dz}$$

$$[\mathbf{D}_{tb}^{t}] = \int_{h_3}^{h_4}[\mathbf{C}_b]_m \left[1+\left(\frac{E_c}{E_m}-1\right)V^{(3)}\right]\mathrm{dz},$$

$$[\mathbf{D}_{trb}^{t}] = \int_{h_3}^{h_4}[\mathbf{C}_b]_m \left[1+\left(\frac{E_c}{E_m}-1\right)V^{(3)}\right][\mathbf{Z}_3]\mathrm{dz},$$

$$[\mathbf{D}_{ts}^{t}] = \int_{h_3}^{h_4}[\mathbf{C}_s]_m \left[1+\left(\frac{E_c}{E_m}-1\right)V^{(3)}\right]\mathrm{dz}$$

$$,[\mathbf{D}_{trs}^{t}] = \int_{h_3}^{h_4}[\mathbf{C}_s]_m \left[1+\left(\frac{E_c}{E_m}-1\right)V^{(3)}\right][\mathbf{Z}_7]\,\mathrm{dz},$$

$$\left[\mathbf{D}_{rrb}^{b}\right] = \int_{h_3}^{h_4}[\mathbf{Z}_3]^T[\mathbf{C}_s]_m \left[1+\left(\frac{E_c}{E_m}-1\right)V^{(3)}\right][\mathbf{Z}_3]\,\mathrm{dz},$$

$$[\mathbf{D}_{rrs}^{b}] = \int_{h_3}^{h_4}[\mathbf{Z}_7]^T[\mathbf{C}_s]_m \left[1+\left(\frac{E_c}{E_m}-1\right)V^{(1)}\right][\mathbf{Z}_7]\,\mathrm{dz}$$

$$[\mathbf{D}_{ts}^{b}] = \int_{h_0}^{h_1}[\mathbf{C}_s]_m \left[1+\left(\frac{E_c}{E_m}-1\right)V^{(1)}\right]\mathrm{dz},$$

$$[\mathbf{D}_{ts}^{t}] = \int_{h_0}^{h_1}[\mathbf{C}_s]_m \left[1+\left(\frac{E_c}{E_m}-1\right)V^{(3)}\right]\mathrm{dz},$$

$$[\mathbf{D}_{ts}^{c}] = 2[\mathbf{C}_s^{c}]h_c\,,\ [\mathbf{D}_{ts}^{v}] = [\mathbf{C}_s^{v}]h_v\,,\ \left[\mathbf{D}_{ts}^{p}\right] = \left[\mathbf{C}_s^{p}\right]h_p$$

$$\left[\mathbf{D}_{tbs}^{p}\right] = \left[\mathbf{D}_{bs}^{p}\right]h_p,\ \ \left[\mathbf{D}_{trbs}^{p}\right] = \int_{h_5}^{h_6}\left[\mathbf{C}_{bs}^{p}\right][\mathbf{Z}_{10}]\mathrm{dz},$$

$$\left[\mathbf{D}_{rtbs}^{p}\right] = \int_{h_5}^{h_6}[\mathbf{Z}_5]^T\left[\mathbf{C}_{bs}^{p}\right]\mathrm{dz}$$

$$\left[\mathbf{D}_{rrbs}^{p}\right] = \int_{h_5}^{h_6}[\mathbf{Z}_5]^T\left[\mathbf{C}_{bs}^{p}\right][\mathbf{Z}_{10}]\mathrm{dz},\ [\mathbf{D}_{trb}^{c}] = \int_{h_2}^{h_3}[\mathbf{C}_b^{c}]\,[\mathbf{Z}_2]\mathrm{dz}$$

$$[\mathbf{D}_{trb}^{v}] = \int_{h_4}^{h_5}[\mathbf{C}_b^{v}]\,[\mathbf{Z}_4]\mathrm{dz},\ \left[\mathbf{D}_{trb}^{p}\right] = \int_{h_5}^{h_6}\left[\mathbf{C}_b^{p}\right][\mathbf{Z}_5]\mathrm{dz}$$

$$[\mathbf{D}_{rrb}^{c}] = \int_{h_2}^{h_3}[\mathbf{Z}_2]^T\left[\mathbf{C}_{bs}^{p}\right][\mathbf{Z}_2]\mathrm{dz},\ [\mathbf{D}_{rrb}^{v}] = \int_{h_4}^{h_5}[\mathbf{Z}_4]^T\left[\mathbf{C}_{bs}^{p}\right][\mathbf{Z}_4]\mathrm{dz},$$

$$\left[\mathbf{D}_{rrb}^{p}\right] = \int_{h_5}^{h_6}[\mathbf{Z}_5]^T\left[\mathbf{C}_{bs}^{p}\right][\mathbf{Z}_5]\mathrm{dz},\ [\mathbf{D}_{trs}^{c}] = \int_{h_2}^{h_3}[\mathbf{C}_s^{c}]\,[\mathbf{Z}_7]\mathrm{dz},$$

$$[\mathbf{D}_{trs}^{v}] = \int_{h_4}^{h_5}[\mathbf{C}_s^{v}]\,[\mathbf{Z}_9]\mathrm{dz},\ \left[\mathbf{D}_{trs}^{p}\right] = \int_{h_5}^{h_6}\left[\mathbf{C}_s^{p}\right][\mathbf{Z}_{10}]\mathrm{dz},$$

$$[\mathbf{D}_{rrs}^{c}] = \int_{h_2}^{h_3}[\mathbf{Z}_7]^T[\mathbf{C}_s^{c}][\mathbf{Z}_7]\mathrm{dz},\ [\mathbf{D}_{rrs}^{v}] = \int_{h_4}^{h_5}[\mathbf{Z}_9]^T[\mathbf{C}_s^{v}][\mathbf{Z}_9]\mathrm{dz},$$

$$\left[\mathbf{D}_{rrs}^{p}\right] = \int_{h_5}^{h_6}[\mathbf{Z}_{10}]^T\left[\mathbf{C}_s^{p}\right][\mathbf{Z}_{10}]\mathrm{dz}$$

$$\left\{\mathbf{D}_{tb}^{p}\right\} = -\int_{h_5}^{h_6}\{\mathbf{e}_b\}\Big/h_p\ \mathrm{dz},\ \left\{\mathbf{D}_{ts}^{p}\right\} = -\int_{h_5}^{h_6}\{\mathbf{e}_s\}\Big/h_p\ \mathrm{dz},$$

$$\left\{\mathbf{D}_{rb}^{p}\right\} = -\int_{h_5}^{h_6}[\mathbf{Z}_5]^T\{\mathbf{e}_b\}\Big/h_p\ \mathrm{dz}$$

$$\left\{\mathbf{D}_{rs}^{p}\right\} = -\int_{h_5}^{h_6}[\mathbf{Z}_{10}]^T\{\mathbf{e}_s\}\Big/h_p\ \mathrm{dz}.$$